b-Meson Tracking at LHCb: a Feasibility Study

Jan IJsbrand Rol

March 2021

Reading committee

First examiner:	Dr. ir. C.J.G. Onderwater
Second examiner:	Dr. J. G. Messchendorp
Daily Supervisor:	Dr. M. C. van Veghel

Contents

Introduction

"There is nothing new to be discovered in physics now. All that remains is more and more precise measurement" is a quote falsely attributed to Lord Kelvin, who passed in 1906. Instead, it was Albert A. Michelson who stated that: "... the future truths about physical science are to be looked for in the sixth place of decimals" [1]. In 1905, Albert Einstein published a paper on the photoelectric effect, advancing the hypothesis that light interacts as quantized packets of energy, rather than waves, laying part of the foundation of what would later become quantum theory. Lord Kelvin might just have read it.

Physics turned out to be far from complete. As a coherent picture of quantum physics started to emerge, arguably more open questions in physics came up than ever before. Over the course of the 20^{th} century the physics community has been playing catch-up. Still, physics is by no means in the state that Michelson thought it was at the turn of the previous century. The model that has been developed is very successful in predicting a wide range of physical phenomena in particle physics. Nonetheless, the general consensus is that this model—The Standard Model (SM)[2]—is not complete; several profound questions remain[3, 4].

The Large Hadron Collider under Geneva has been constructed with the purpose of finding answers to some of those questions. The LHCb is uniquely equipped to shed light on an active area of research called the 'flavour puzzle'. The particles predicted in the Standard Model come in different types, or flavours if you will. These flavours transition into one another at unexplained rates. Additionally, the flavours seem to order themselves in a mass hierarchy comprising three generations. The Standard Model provides no account for the origin of these phenomena. As such, better understanding the flavour puzzle could provide hints for physics beyond the Standard Model.

Recent measurements have suggested that the heavier particle flavours couple more strongly to possible New Physics (NP)[5]. The LHCb experiment is one of the four major experiments positioned around the LHC, and is designed specifically to detect the heavier particle flavours. The detector has already achieved considerable success, but will provide a remarkable improvement in recorded luminosity—a measure for the amount of collision events—once the upgrade which it is currently going through is complete. And

with the upgrade a novel method of using the LHCb detector perhaps becomes feasible.

The feasibility study discussed here proposes the analysis of the $B_c^+ \to \tau^+ \nu_\tau$ decay mode with the LHCb experiment. A measurement of the branching fraction of this channel could provide insight into an existing problem in particle physics from a different angle. This is elaborated on in the first chapter. To perform the analysis, a new detection tool is introduced that is utilized in combination with the existing measurement apparatus. The tool has been created to detect the hits from charged *b*-mesons in the VELO sensor which is primarily used to locate the collision vertices. The tool is capable of determining the direction of the meson directly while this is normally inferred from the decay products of the meson. The additional information can contribute greatly to the analysis of the intended decay modes, which so far have not been measured at LHCb. The work presented in the following pages is a study of **the feasibility of an analysis of the decay of charged *b*-mesons into a tauon with the LHCb experiment and what the benefit is of utilizing the novel B-Tracking Tool.**

The first chapter will introduce the theoretical framework that so far has only been covered in general terms. This will also provide part of the motivation for the specific decay modes at hand. Chapter 2 will give an overview of the LHCb detector including a short discussion of the methodology of the B-Tracking Tool. Chapter 3 will cover several different—but closely related—subjects: the rest of the motivation for what will be our 'signal' decay modes; the identification of the expected background modes; simulation methods; and first estimates for the resulting yields and efficiencies of the analysis. Chapter 4 is the first of two chapters that lay out a selection strategy. Chapter 4 will deal with the specific background modes identified in the previous chapter. Combinatorial background—random combinations of noise and hits—is typically a continual nuisance in studies at the LHC. The final chapter will explore combinatorics in a B-Tracking analysis.

Chapter 1

The Standard Model: Probing Lepton Flavour Universality

Although starting an introduction to modern physics with the teachings of Democritus and the first conception of the indivisible 'atomos' is tempting to emphasize how far physics has come, it would be a gross undervaluation of the rapid progress in physics of the last century or so[6]. After an interpretation of quantum physics could be agreed upon by most of the physics community in the first decades of the 20^{th} century, nature started to reveal itself on smaller scales and at higher energies. The theoretical and experimental sides of what is now known as the Standard Model, emerged together; gauge theories on the one hand provided an explanation for the different interactions observed in nature, while on the other hand particles—some predicted by those theories—were observed for the first time. The pieces fit together in what is now called the Standard Model of particle physics. The Standard Model incorporates three of the four known fundamental interactions: the strong, the weak and the electromagnetic interaction. These interactions are felt by a set of particles divided in two types: bosons with an integer spin and fermions with half-integer spin.

The fermions can be further divided into three generations of increasing mass. Each generation is composed of two quarks, an 'up'-type quark with electric charge $+\frac{2}{3}e$ and a 'down'-type quark with electric charge $-\frac{1}{3}e$, one negatively charged lepton and a corresponding neutral lepton-neutrino. For each of the particles in the Standard Model, a corresponding anti-particle with opposite quantum numbers exists. In the Standard Model the particles interact with three gauge fields. The Gauge bosons are excitations of those fields, and mediate the fundamental interactions. The γ mediates the electromagnetic force, the $W^{\pm}$ and Z^0 bosons the weak interaction and the 8 gluons, denoted g, the strong interaction. The Higgs field couples to most of the particles to give them mass, excluding the photon, gluons and neutrinos. An excitation of the Higgs field is what is known as the

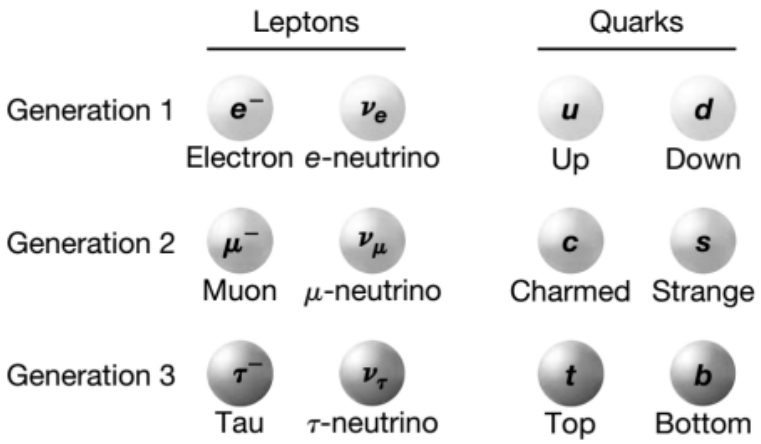

Figure 1.1: The fermions of the Standard Model. There are three generations of increasing mass, where each generation contains a lepton with a corresponding neutrino and an up- and down-type quark. Antiparticles are not illustrated, but would be denoted with a bar. Illustration from [7].

Higgs boson. An overview of the different fermions of the Standard Model is shown in figure 1.1. One of the cornerstones of the Standard Model is the indifference of the interactions to the lepton flavour: leptons are treated equally by all three interactions, which is called lepton flavour universality, or LFU in short.

Most of the particles of the framework just described are unstable and typically do not form compositions, but quarks tend to clump together in what is called hadronic matter. Baryons contain an odd number of quarks—typically three—forming the basis of matter around us. Protons and neutrons are the most common examples of baryons. Mesons are particles consisting of a quark and an anti-quark. In flavour physics, the focus has been on mesons with at least one of the heavier quarks. The heaviest quark determines the capital symbol, while a second flavoured quark is given in subscript. For example, B_c^+ is a $\bar{b}c$ pair and D_s^- stands for a $c\bar{s}$ pair.

The Standard Model has been extremely successful in predicting the behaviour of nature over the full breadth of particle physics. Its success is not boundless however. The theory of gravity, general relativity, has so far resisted a description within the same framework as the Standard Model; quantum field theory. Other difficulties remain; why nature has chosen to present itself in three generations remains a mystery. Why neutrinos have mass—which is why they seem to oscillate into each other—is another such question the Standard Model has no answer to [4]. And new measurements are made that are at odds with the predictions of the Standard Model.

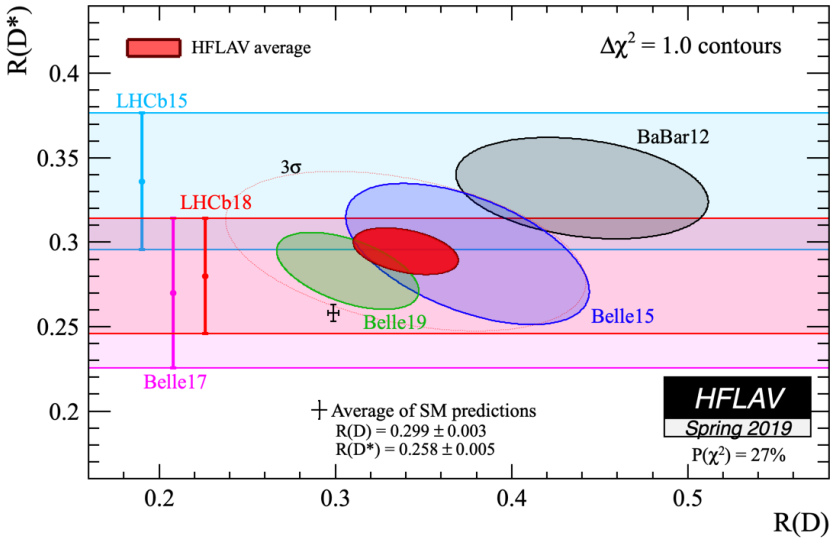

Figure 1.2: Two-dimensional fit of the $R(D)$ and $R(D^*)$ branching fraction measurements which shows a combined deviation of roughly 3σ with the SM prediction.

1.1 Violations of LFU

One recent example of tension with Standard Model predictions is found in heavy meson decays. Lepton flavour universality is typically tested by comparing branching ratios of decays that differ only in lepton flavour. LFU defines these ratios precisely, as all lepton flavours would share the same coupling constant. The tension has emerged over the last decade or so in $b \to s l^+ l^-$ and $b \to c l \nu_l$ decays, where b, s and c are single quarks as the spectator quark is omitted [8]. The $b \to c l \nu_l$ interaction has been measured in neutral b-meson decays by 'B-factories' Belle and Babar, and later also at LHCb[5]:

$$R(D^*) = \frac{\mathcal{B}(\overline{B}^0 \to D^{*+} \tau^- \overline{\nu}_\tau)}{\mathcal{B}(\overline{B}^0 \to D^{*+} \mu^- \overline{\nu}_\mu)}$$

and is found to be 2.1σ removed from the Standard Model prediction. This measurement corroborated findings at other experiments, for several different decays—including the unexcited state of the c-meson, D^+—for a combined tension of between 3 and 4σ [8]. The fact that these results have been found for different decays is a sign that this is not due to a measurement error, but to some physics that is not part of the Standard Model—often dubbed 'beyond' the Standard Model, or BSM.

If the current trend in flavour physics continues, the tension with Standard Model

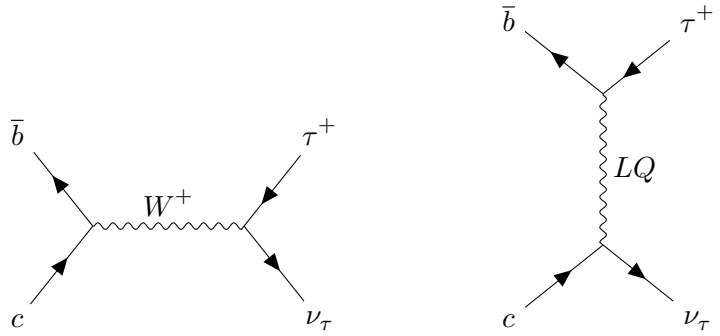

Figure 1.3: The $B_c^+ \to \tau^+ \nu_\tau$ decay mediated by a W^+ boson as predicted by the standard model(left), and the decay mediated by a New Physics Leptoquark (right).

predictions will increase past the point of a 5σ deviation. In that case the tension can rightfully be called a discovery of new physics, and the question remains what is the cause behind the deviation. Several theoretical explanations have been proposed that involve new particles, notably the Leptoquark—proposed much earlier than the first signs of LFU violation—and an additional (number of) gauge boson(s), that couple more strongly to the heavier generations of leptons [9, 10]. These new particles are predicted to be in the TeV/c^2 range. As such, they cannot produced at the LHC in meaningful numbers. However, they can contribute virtually to the interactions that are currently showing deviations from LFU predictions.

1.2 $bc \to l\,\nu_l$ decays

To further understand possible lepton flavour non-universality, other decays involving $b \to s\,l^+l^-$ and $b \to c\,l\,\nu_l$ interactions are sensible candidates. Of special import to this thesis is the $bc \to l\,\nu_l$ transition. On the particle level, it is subject to the same four-point interaction as the $R(D^{(*)})$ measurements, but the particle order differs. Rather than a b quark transitioning into a c quark and two leptons, the two quarks annihilate and form two leptons: $bc \to l\,\nu_l$. The interaction takes place in the $B_c^+ \to \tau^+ \nu_\tau$ decay, which motivates the intended analysis. The standard model diagram as well as one mediated by a Leptoquark are shown in figure 1.3.

In describing the four-point interaction with b, c, l, and ν_l it is common practice to define an effective field theory. In the effective field theory, interactions mediated by particles much heavier than those taking part in the decay are integrated out. The effective

Hamiltonian describing the interaction can then be written as [11]:

$$\mathcal{H}_{\text{eff}} = \frac{4G_F}{\sqrt{2}} V_{cb} \left[(1 + \mathcal{C}_{V1})\mathcal{O}_{V1} + \mathcal{C}_{V2}\mathcal{O}_{V2} + \mathcal{C}_{S1}\mathcal{O}_{S1} + \mathcal{C}_{S2}\mathcal{O}_{S2}\right] + \text{h.c.}, \tag{1.1}$$

where G_F is Fermi's constant, V_{cb} the 6$^{\text{th}}$ CKM matrix element [12] and h.c. stands for the hermitian conjugate terms. The CKM matrix is a unitary 3x3 matrix describing the flavour mixing of quarks mediated by the weak force. Although it is close to diagonal, meaning transitions predominantly happen within the particle generations (like $c \to s$), the off-diagonal components are non-zero. The determination of the matrix elements is an active area of research at LHCb and elsewhere.

$\mathcal{C}_i$ and $\mathcal{O}_i$ in equation 1.1 are the Wilson coefficients and operators, respectively. The operators contain the long-range, non-virtual effects determined by the initial and final state of the transition. The coefficients contain the short distance perturbative effects that would be expected from new physics effects such as the leptoquark and extra gauge bosons described above. $\mathcal{O}_{V1}$ Is the only operator present in the Standard Model. A result showing a deviation from LFU could validate existing signs of new physics in the same four-point interaction. However, the $b \to c l \nu_l$ transition is more sensitive to Vector – Axial-vector interactions, included in $\mathcal{C}_{V1,2}$, but $bc \to l\,\nu_l$ is much more sensitive to the scalar interactions, in $\mathcal{C}_{S1,2}$. Several proposed new physics explanations for LFU violation contribute to these scalar interactions. As such, results in the latter transition can not only corroborate LFU violation findings, but also probe different contributions in the effective Hamiltonian, which will in turn shed light on the nature of the new physics that could be responsible.

Chapter 2

The LHCb Detector

In order to probe the Standard Model, a large accelerator complex has been built near Geneva, Switzerland. Although originally electrons and positrons circled the 27 km that span the main ring where the LHC is now operating, the main purpose is to detect proton-proton collisions at up to 14 TeV center-of-mass energies. Along the ring, 4 main interaction regions have been designed where the two opposing particle beams collide. ATLAS[13] and CMS[14] are two general purpose detectors, designed with the purpose of among other things, finding the Higgs boson which was achieved in 2012 [15]. ALICE[16] is designed specifically to measure heavy ion collisions. The LHCb experiment[17] is smaller than its cousins and is designed to precisely measure *c*- and *b*-meson decays produced in proton-proton collisions. Contrary to the other detectors, LHCb is a single-arm forward spectrometer meaning that only to one side of the interaction point measurements are taken. The angular coverage of the detector is also different; whereas the other three detectors observe lower pseudorapidity ranges, LHCb covers $2 < \eta < 5$, where $\eta = -\ln\left[\tan\left(\frac{\theta}{2}\right)\right]$, roughly corresponding to an angle θ of 1 to 15 degrees with respect to the beam axis. A large fraction of heavy mesons is produced in this angular region. The detector is designed to accurately determine the kinematic characteristics and flavour of the charged particles that are the decay products of these heavy mesons.

Sitting some millimeters from the interaction region, the VErtex LOcator (VELO) is composed of a set of sensors that detect the large number of hits from charged particles, from which their tracks are reconstructed. In order to determine the momentum of charged particles, tracking stations are positioned before and after a dipole magnet. The curvature of the inferred track provides a measure of its momentum. To differentiate between particle species—and by extension their mass—ring-imaging Cherenkov (RICH) detectors measure the angle of emitted Cherenkov radiation, which is translated to the particle velocity. Neutral particles cannot be traced the same way as charged particles are, but the energy deposits of all particles can be measured, which is the function of the elec-

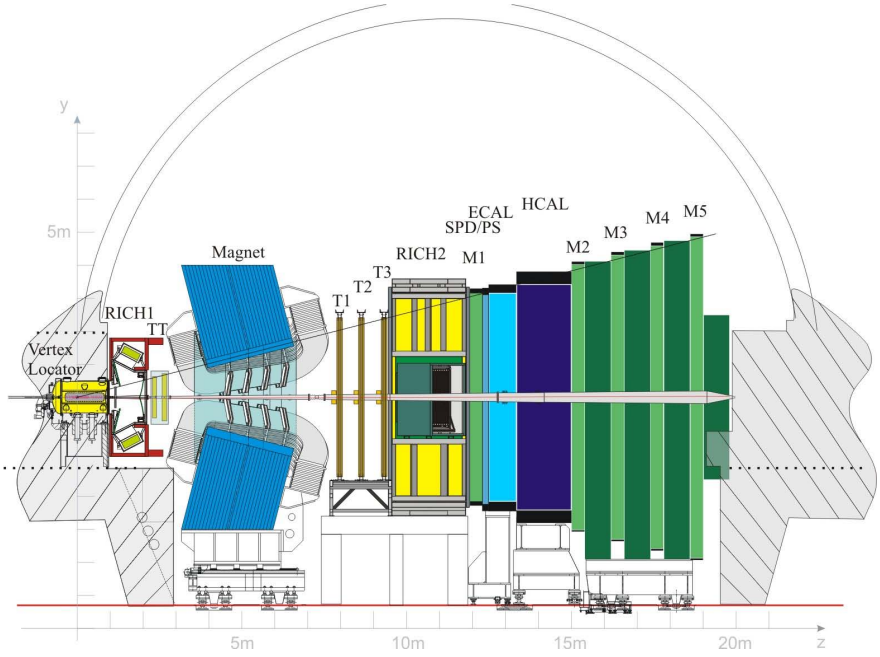

Figure 2.1: Schematic of the LHCb detector. From left to right: the VELO, the Cherenkov ring imaging detectors (RICH1, RICH2), the magnet and the tracking stations (TT, T1-T3), the muon stations (M1-M5) and the calorimeter system (ECAL, HCAL).

tromagnetic and hadronic calorimeters (ECAL & HCAL). Finally, many of the less reactive muons make it through most of the detector material unscathed and are subsequently detected in the muon stations at the far end of the detector. The huge stream of information that is produced during data taking has to be reduced to a rate more than a thousand times smaller. The trigger system, consisting of one hardware and two software stages, rejects almost all uninteresting events and brings the data stream down to workable levels. Most components of LHCb are being upgraded or replaced at the time of writing such that an almost entirely new detector is commissioned for the start of run 3, which is currently scheduled for April 2022. This leads to an improvement of many aspects of the proposed analysis and is of special import to the VELO sensor.

This chapter will cover the different components of the detector in order, i.e. starting from the interaction point. As such, the Vertex Locator, or VELO, is treated first and more extensively than the other components because the B-Tracking tool methodology is based solely on the information the VELO modules provide. Moving outward from the VELO sensors, the other components will be discussed shortly. Finally, the software aspect of LHCb is touched upon and more specifically the B-Tracking tool is described including the resolution it provides.

2.1 Hardware

The physical components of the LHCb detector are discussed, to provide an overview of how information is being gathered.

Vertex Locator

The Vertex Locator is a tracking detector that measures the hits from charged particles flying through the individual sensors. It is the most precise detector in the LHCb detector which is necessary, as the different particle tracks are packed closely together close to the interaction region. The main purpose of the VELO is to determine the position of the collision(s) of the opposing beams—the primary vertices (PV)—from which all other particles originate and the secondary vertices (SV) to allow for accurate decay time measurements of b- and c-mesons. The vertex locator is an essential component of the detector as it allows for the determination of the impact parameter, or IP, of subsequent tracks. The IP is defined as the shortest distance from the track to the closest PV. A sizeable IP points at a heavy meson decay as the lifetime of b- and c-mesons causes the displacement of ensuing particle tracks.

The entire VELO detector comprises 42 sensors that are placed every 3 centimeters along the interaction region. The sensors are retracted when the proton bunches are injected, accelerated and stabilized. When the beams are focused and start to collide, the modules move inward, to only 8 millimetres from the beam axis. The upgraded VELO includes 10 extra sensors for a total of 52 and will provide improved resolution. The distance from the beam axis is reduced to only 5.1 millimetres. Short-lived particles like heavy mesons are therefore much more likely to reach the active region of the VELO—between the inner and outer edges of the VELO sensors—with the upgraded VELO configuration. This is reflected in the results obtained in the next chapter.

Other detector components

Although the primary goal of the VELO is to localize the PVs, it is also part of the entire tracking system. A second tracking station is positioned right before the magnet, the TT. It can be used to get a preliminary estimate on the momentum of the particles passing through, as the magnetic field has a non-zero value around the TT. After the magnet, the main set of tracking stations, T1 through T3 are placed to accurately measure the curvature of the tracks and to match them with hits in the VELO and possibly the TT to obtain a so called "long track". The main stations are comprised of both silicon strip detectors closer to the beam pipe to untangle the high density of hits, and cost-effective straw tubes filled with gas farther away from the beam pipe called the inner and outer tracker, respectively.

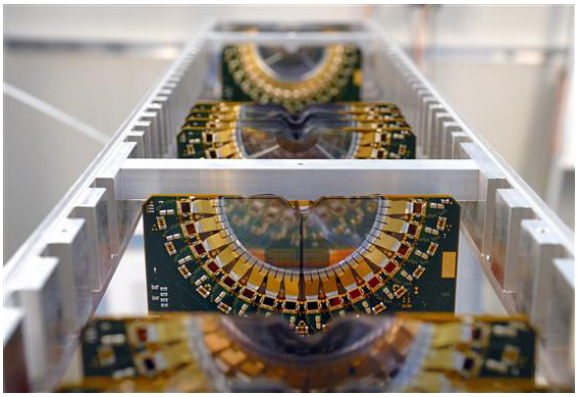

Figure 2.2: Photo of a number of the 42 VELO sensors along the beam pipe. From the LHCb public webpage.

Cherenkov radiation is generated when charged particles move faster than light does through a dielectric medium. The radiation is emitted at an angle from the flight direction proportional to the particles speed. Together with the obtained momentum the particle's mass can be determined, and hence the type. The first ring imaging Cherenkov detector, RICH1, sits before the magnet and is geared to measure lower momentum particles, while the detector behind the magnet, RICH2, is focused on measuring the higher momentum particles that typically stay closer to the beam axis.

The calorimeters are designed to stop all particles smashing into the metal plates sandwiched between detector plates. Both neutral and charged particles interact with the dense metal and create a particle shower that travels through to the detector plates in between. The size of the shower is directly proportional to the energy deposited in the calorimeter, producing a measure for the energy of the initial particle. The Scintillating Pad Detector (SPD) and the Pre-Shower detector (PS) perform an initial particle classification, while the electromagnetic calorimeter and the hadronic calorimeter measure the energies of electromagnetic and hadronic particles, respectively.

Not many particles make it past the calorimeters, but when one does, it is usually a muon. Therefore the final region at the end of the detector houses five muon stations. The stations are responsible for providing fast identification of passing muons. The presence of relativly high transverse momentum muons is a strong indication of b-meson decays, therefore hits in the muon station are an integral part of the trigger system discussed next.

2.2 Software

Although the physical components are commonly referred to as the detector, the software is a just as important part of the experiment. The programs responsible for the recon-

struction of tracks and vertices, determining whether to save events and more are legion. We will shortly discuss the trigger system that is now completely software based, before talking about the reconstruction of b-meson tracks specifically. Simulation is another part of the LHCb software, but is discussed in the next chapter.

Trigger

The trigger is not only discussed because it is an integral part of the detector, but also because one of the first steps towards the intended analysis will be the introduction of a new trigger line. The trigger originally consisted of three levels, the hardware trigger `L0` and the two software levels called the high level triggers, `HLT1` and `HLT2`. With the upgrade of the LHCb detector, the collision rate is expected to be five times greater. As such, the trigger has to evolve with it, to keep up with the increased stream of data and better data selection. Therefore, `L0` will be discarded and only the software stage remains. The reconstruction of the events will take place in real-time, and is done completely for all events. A first geometric and kinematic selection is made, after which the calibration of the detector is necessary to determine precision particle identification and track quality to further reduce the datastream while still producing a total of some 2-5 GB/s written to storage.

2.2.1 B-Tracking Tool

The software that performs the reconstruction is not discussed as it is entirely out of the scope of this research. However, the novel addition to the selection software that is the starting point of this study is. Normally, reconstruction of two types of objects take place: tracks and subsequent vertices. The process starts in the VELO, where straight sequences of hits in the modules are detected. Some of the line segments point to the same point, which allows for the reconstruction of one or more primary vertices, where a proton-proton collision is expected to have happened. Additionally, the line segments are then continued downstream in what is called "forward tracking", when additional hits are searched for in the main tracking stations before and after the magnet. Combined with information from the other components of the detector, the (pseudo-)stable particles are identified. On the basis of these final state particles, the presence of short-lived particles is inferred, like c- and b-mesons. This approach is commonplace in high energy experiments, and is successfully unravelling the mystery of heavy mesons.

In some cases, information is lost with the current methodology. If the hits in the VELO sensors do not provide additional hits when followed through to the tracking stations, the hits are only used in the determination of the PVs. But if it turns out that one of the segments from the primary vertex to a hit is produced by a parent particle the final

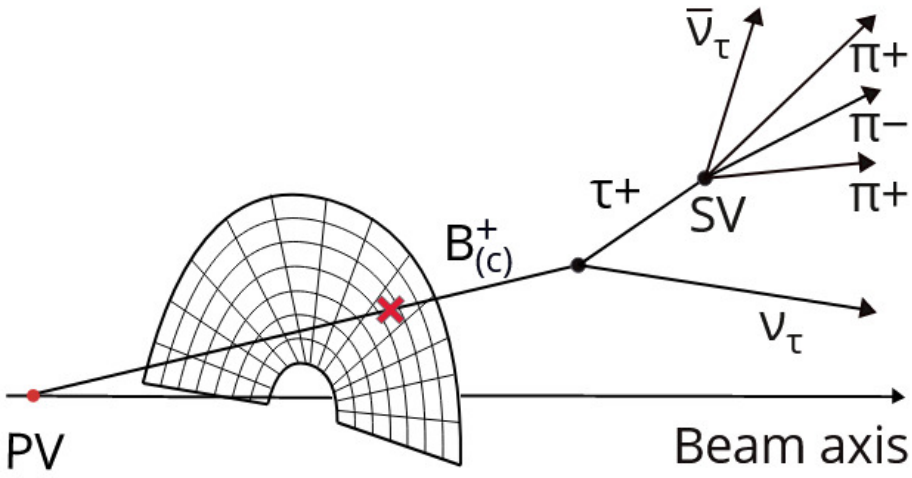

Figure 2.3: A *b*-meson leaving a hit in a VELO sensor before decaying into a pion triplet via a tau lepton. Along the line between the PV and the SV, the B-Tracking Tool searches for VELO hits.

state of which is selected as a signal event, it holds important information on the direction of the parent. The reason why no attempt is made to retrieve the information is simple; *c*- and *b*-mesons typically fly a centimeter or so before decaying, while—even under favourable run 3 conditions—the first VELO sensor requires at least ten times that flight distance to get to.

Consider the B^+ meson. Its mean lifetime is reported by the PDG to be 1.638 ps [18]. Assuming a velocity equal to the speed of light, one lifetime corresponds to a flight distance of half a millimeter. However, the decay of elementary particles is an unpredictable process. Reported lifetimes are actually mean lifetimes. Thus, there is a $1/e$ probability that an individual B^+ meson has not decayed yet after one mean lifetime. Even after several lifetimes, a small fraction of B^+ mesons survive. When including the effects of time dialation, the probabilistic nature of decays allows a small fraction of B^+ mesons to move far enough to leave a trace in the nearest VELO sensor(s). This is also why the upgrade of the VELO plays a crucial role in the motivation for this study; moving the sensors closer to the crossing beams drastically increases the fraction of *b*-mesons hitting the subdetector. If a $B^+_{(c)}$ decay is detected on the basis of the final state particles, the decay can be traced back to hits in the VELO, if the meson has not decayed prematurely. This is exactly what B-Tracking aims to do: for identified charged *b*-meson decays—as neutral particles do not trigger VELO hits—infer the direction of the meson when it has left one or more hits in the VELO.

The B-Tracking tool is run as part of the reconstruction procedure and evaluates the

raw VELO data. In the following chapter, the choice for a $B^+_{(c)} \to \nu_\tau \tau^+ (\to \pi^+\pi^-\pi^+\overline{\nu}_\tau)$ decay analysis is motivated, but let's take the example here to illustrate the process that takes place when running the B-Tracking tool. A sketch of an example decay is shown in figure 2.3. First of all, signal data is selected on the reconstructed final state of the decay; the pion triplet. The primary vertex from which the decay most likely has originated has also been reconstructed. The three pions are traced back to a common point of origin called the secondary vertex (SV). The secondary vertex is essential to create a search window that is narrow enough to suppress noise. A straight line from the PV to the SV indicates the path along which the B-Tracking tool searches for hits in the VELO sensors that are close enough to the line. The proximity is defined by requiring a maximum value for the χ^2 of including the hit in the fitting of the track from the PV to the SV. For the results obtained throughout the study, $\chi^2 < 16$ is taken, although the value striking the balance between efficiency and accuracy is a matter of optimization. If at least one VELO hit is found, the event is flagged and the number of hits reported under `Bp_BpTracking_nHits` in the resulting ntuple. If one VELO hit is found, the direction of the meson is determined. If more than one VELO hit is found, at least three coordinates—including the PV—are available, so a full track fit is performed.

This example also illustrates where the B-Tracking Tool can contribute. Decays without an intermediate particle do not benefit much from the tool: the direction of the meson can be inferred accurately from the PV-SV path. For a decay with an intermediate particle like the τ in the example, the meson direction is normally still inferred from this path. However the 'kink' produced by the intermediate particle sabotages an accurate meson direction determination. Therefore, decay channels where the decay vertex of the particle of interest is not reconstructible, does the B-Tracking Tool provide unique information.

An objection to the method just described would be the indifference with which the tool records VELO hits. Any charged particle happening to pass through the VELO sensor around the PV-SV line segment can trigger a B-Tracking hit. This is especially troublesome for charged particles that originate from the decaying *b*-meson. In the example, the tau or even one of the pions—as the SV resolution is not perfect—can leave VELO hits that are attributed to the heavy meson. The final chapter will deal with this issue to some extent. For now, it is important to be aware that this is a first version of the B-Tracking Tool. All results presented throughout this study have been obtained with this first version. Some aspects of the tool can be optimized, and should be as one of the next steps forward. This is not our aim here.

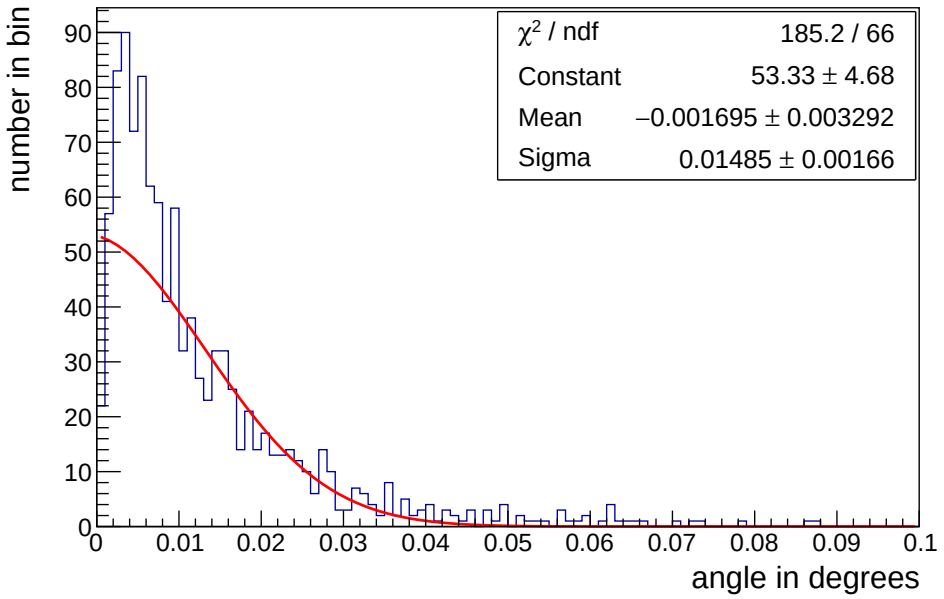

Figure 2.4: Distribution of the angle between the 'true' Monte Carlo B^+ direction and the reconstructed direction of the B-Tracking tool. A Gaussian centered around 0 is fit and the standard deviation used in subsequent simulations.

Resolution

A final note is in order regarding the accuracy of the B-Tracking Tool. As part of the conducted research relies on large simulated datasets that do not include the detector response, the B-Tracking Tool is not actually applied on this data, but rather the response of the tool is estimated and taken into account as if it would have been applied. To this end, it is necessary to quantify the precision the tool delivers. A separate dataset has been simulated over which the tool *is* run. Chapter 3 will cover simulation methods in more detail, but for now it will suffice to say that the simulated data consists of the original simulated objects rather than smeared or reconstructed objects. As such, a comparison of the flight directions from simulated data and B-Tracking provides a measure of the error on the B-Tracking direction. Figure 2.4 shows the distribution of the angle between the two directions. Approximately thrice the standard deviation—1 millirad—is subsequently used in analysis when the response of the tool has to be taken into account, to compensate for outliers that are not included in the fit but ostensibly worsen the accuracy of the tool.

Chapter 3

Roadmap to a B-Tracking analysis: Signal, Background, Simulation and Estimates

In the first chapter the potential of measuring the branching ratio of the $B_c^+ \to \tau^+\nu_\tau$ decay has been laid out. Other considerations are in order to translate the theoretical interest into a well-formulated intent of research that is possible with the LHCb experiment. To do so, it is informative to perform some 'back of the envelope' calculations of the number of B-Tracking hits that can realistically be expected in a future analysis. To get to that point, several choices regarding signal channels, background channels and the simulation method have to be made. The B-Tracking feasibility study presented in the coming chapters concerns the $B^+_{(c)} \to \nu_\tau\tau^+(\to \pi^+\pi^-\pi^+\overline{\nu}_\tau)$ decays. This decision is motivated in the first section, as well as the benefit of considering the $B^+ \to \nu_\tau\tau^+(\to \pi^+\pi^-\pi^+\overline{\nu}_\tau)$ decay as a signal channel. Only when background events are controlled adequately, an analysis of these decays is possible. Given the signal decay channels, other background channels must therefore be identified that can masquerade as a signal event, which is the subject of section 2. To study both signal and background to determine an effective signal selection strategy, simulated data is necessary. Section 3 covers the different simulation methods considered. When these preparations are in order and the intended research is well-formulated, a first estimate produces a viable number of signal and background events triggering a 'B-Tracking hit', demonstrating that the study is in principle possible.

3.1 Signal decay channels

When probing the interaction discussed in chapter 1, i.e. $B_c^+ \to \ell^+\nu_\ell$, the B_c meson that comprises b and c quarks can decay into any of the three leptons. Previous findings show signs that flavour violating effects couple to the heavier lepton families. Naturally, a tauonic decay channel would be preferable. It is important to keep in mind the goal is a measurement of the branching fraction of decaying directly into a lepton. The $B_c^+ \to \nu_\tau\tau^+(\to \mu^+\nu_\mu)$ decay therefore contributes to a $B_c^+ \to \tau^+\nu_\tau$ measurement and not a $B_c^+ \to \mu^+\nu_\mu$ measurement. Additionally, the other two lepton types—muons and electrons—make a very difficult event to reconstruct, as they are (pseuo-)stable particles and a single lepton does not enable an adequate secondary vertex determination. A tau lepton on the other hand, has a very short lifetime and therefore the decay products rather than the lepton is measured [18]. This brings us to the pion triplet, which is the chosen final state of the intended signal channels. The three pions are all charged and stable enough to be reconstructed. Having three final state particles rather than one makes for a strong SV resolution. Additionally, a more stringent selection criterion can be applied. These considerations combined make it the preferable final state even though it is not the dominant decay mode of the τ.

A different concern is the expected number of decay events over the course of run 3. Given the small production rate of B_c^+-mesons with respect to B^+-mesons combined with the low efficiency of B-Tracking, the number of expected B_c^+-meson signal decays is limited. Given their relative abundance, B^+-meson decays are also included as signal events. The better statistics as well as the availability of well understood calibration channels like $B^+ \to J/\psi\, K^+$ used in chapter 5, makes B^+ meson decays suitable to see how the B-Tracking Tool is doing in an analysis where results can be confirmed. This first use case would also provide the ability to optimize the tool and understand its limitations. It is also an interesting physics channel in its own right, as some theoretical models predict an increase in branching fraction for $B^+ \to \tau^+\nu_\tau$ of 60% over Standard Model predictions [19]. Furthermore, a measurement of both signal decay channel branching fractions gives the ratio of the two. This allows for a suppression of many systematic uncertainties as they are cancelled out in the fraction. Also, a V_{cb}/V_{ub} measurement could perhaps be done.

In short, the $B_{(c)}^+ \to \nu_\tau\tau^+(\to \pi^+\pi^-\pi^+\overline{\nu}_\tau)$ decay channels are relatively well reconstructible channels within the $bc \to \ell\nu_\ell$ family and potentially provide both a good first use-case for B-Tracking and an impactful analysis opportunity. It will be shown that neither signal channels can be studied nearly as well without the use of the B-Tracking Tool. If the analyses are successful, both measurements contribute to the puzzle of lepton flavour universality.

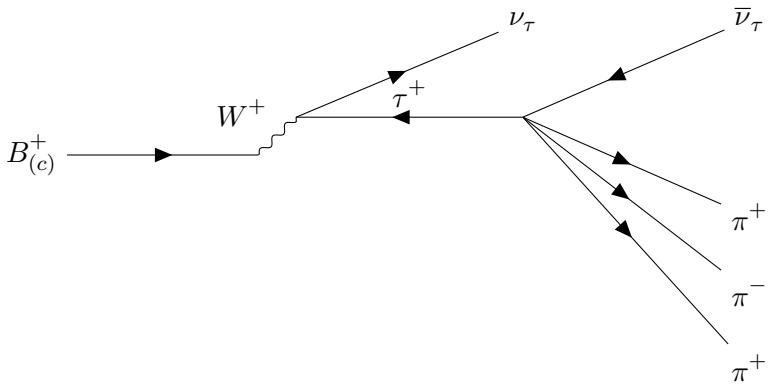

Figure 3.1: Feynman diagram of the signal decay mode. A virtual W^+ boson mediates the meson decay, while the tau lepton is on-shell.

3.2 Background decay channels

The next consideration is that of background events. One of the aims of this study is to determine how to filter unwanted background events to obtain the best signal to background ratio. Signal selection should take place that emphasizes the distinctive features of signal events that are lacking in background events. An overview of the major background contributions is needed to determine what signal events have to be distinctive *from*. Decay channels are primarily separated on the basis of just a few key characteristics. These characteristics are discussed briefly to then identify two major background channels. Note that this choice is by no means exhaustive, rather it is an attempt to select those channels that are relevant at this stage of the analysis. Also note that all considered background channels should be able to leave a B-Tracking hit.

Background channels can be divided into at least four different types. Partially reconstructed, misreconstructed and combinatorial events. Additionally, events that originate from the wrong particle are also a source of background. Partially reconstructed events comprise one or more final state particles that are not reconstructed by the detector. Misreconstructed events in contrast are completely reconstructed but one or more particles is wrongly identified. An example is misidentifying kaons as pions or vice versa.

Before considering possible decay channels, the most prevalent and persistent type of background must first be discussed. Combinatorial background is the result of separate *b*- and or c-meson decays that together accidentally make up the signature characteristics of the signal. As the 'final state' of combinatorial background originates from different vertices, reconstruction of invariant mass as well as other parameters on which a selection is made can yield widely varying results. Some combinatorial background will therefore always pass the selection, regardless of the analysis at hand. In chapter 5 we will deal

with combinatorial background in b-meson decays. The rest of this chapter will tackle specific backgrounds.

Background channels are more likely to be reconstructed as signal events when the following requirements are met:

- **Same reconstructed final state particles**
  First and foremost, decay channels are identified by the observable particles that are produced in the decay. A candidate is not selected if the final state particles do not match the final state of the signal. However, erroneously reconstructed candidates can masquerade as signal events. For example, a $B^+ \to \pi^0 D_s^+ (\to \pi^+\pi^-\pi^+)$ decay mimics the final state of the signal because the D_s^+ is misidentified as a τ^+. However, the presence of the neutral pion provides the opportunity to differentiate this channel from the signal channels.

- **Similar invariant mass of reconstructed end-state particles**
  To identify decay modes by the invariant mass of the combination of observable final state particles is commonplace in particle physics [20, 21]. For signal events, an invariant mass distribution peaking around the rest mass of the parent particle is expected. In our case around 5.28 GeV^2/c^2 and 6.27 GeV^2/c^2 for a B^+ and B_c^+ meson respectively [18]. For this analysis, classification based on invariant mass is more involved since the two neutrinos are not seen by the detector, and their 'missing mass'—more specifically momentum—is 'lost'. Because the invariant mass can be reconstructed to some extent, possible background modes will prove harder to suppress when the initial mass is closer to that of the signal.

- **Same decay topology**
  Background modes can also be identified by their decay topology. By decay topology the structure in terms of vertices and number of decay products of the decay is meant, rather than the particle types or the kinematic parameters. A well known visualization of the decay topology is a Feynman diagram [22]. If the decay topology of a given event does not match that of the signal, strategies are available to determine the difference. An example is the suppression of *prompt* background in an LHCb test of lepton universality[20]. Prompt background has a final state originating from the first decay vertex. The background can be separated from the signal channel which produces the final state only from a secondary vertex by the separation of the two vertices. Differentiation based on decay topologies does require a measurable lifetime of the relevant particles.

- **Relevant branching ratio**
  Since the expected signal yield is low, a fourth requirement should be considered.

Background channels are only relevant given an expected number of background events of the order of 1 or more. Therefore, background channels with relative branching fractions lower than the inverse of the expected yield, can be neglected, assuming reconstruction efficiencies are similar. This fourth requirement,

$$\frac{\mathcal{B}(\text{Background channel})}{\mathcal{B}(\text{Signal channel})} \quad \geq \quad \frac{1}{N_{signal}}, \tag{3.1}$$

is a strong constraint, leaving us with few channels to consider.

At this point, a distinction should be made on the basis of the first item on the list above. Many analyses have to deal with background that does not produce the expected final state. This is both good and bad news. On the one hand, a different final state is a distinctive feature based on which the background can be suppressed. Because of its general nature, efficient methods of dealing with this class of backgrounds are known. An example that has been discussed is the $B^+ \to \pi^0 D_s^+ (\to \pi^+\pi^-\pi^+)$ channel. On the other hand, it is a problem that surely will have to be dealt with. In terms of a feasibility study, a more pressing concern is potential shows-stopping background channels. Figure 3.2 shows the invariant mass distribution of the signal channels. The distributions are smeared because only an estimation of the invariant mass can be made; the two unreconstructed neutrinos obscure a precise invariant mass calculation. This effect—and how B-Tracking might help—is discussed in chapter 4. Given the uncertainty in the invariant mass, an important source of background is charmed meson decays. They might decay in the same manner as the signal channel producing the same final state, while a straightforward distinction cannot be made on the basis of invariant mass. Combined with the relative abundance with which *c*-mesons are produced at the LHC, their decays might pose a serious problem for a B-Tracking analysis.

c-Meson background should therefore be the primary concern. The $D_{(s)}^+ \to \nu_\tau \tau^+ (\to \pi^+\pi^-\pi^+\overline{\nu_\tau})$ decay channels fulfill all requirements except a similar invariant mass, but as can be seen in figure 3.2, this is not a sufficient basis for background suppression. As with the *b*-meson decays responsible for signal events, the anti-particles are also implied whenever $D_{(s)}^+$ decays are considered. With a rest mass of 1.870 GeV/c^2 and 1.968 GeV/c^2 respectively, the D^+ and D_s^+ are much lighter than their *b*-meson counterparts[18]. But the corrected mass distributions of signal events presumably overlap strongly with those of the lighter *c*-mesons. *c*-mesons decaying in the same manner as our signal channel are therefore taken as the background channels to consider in this study.

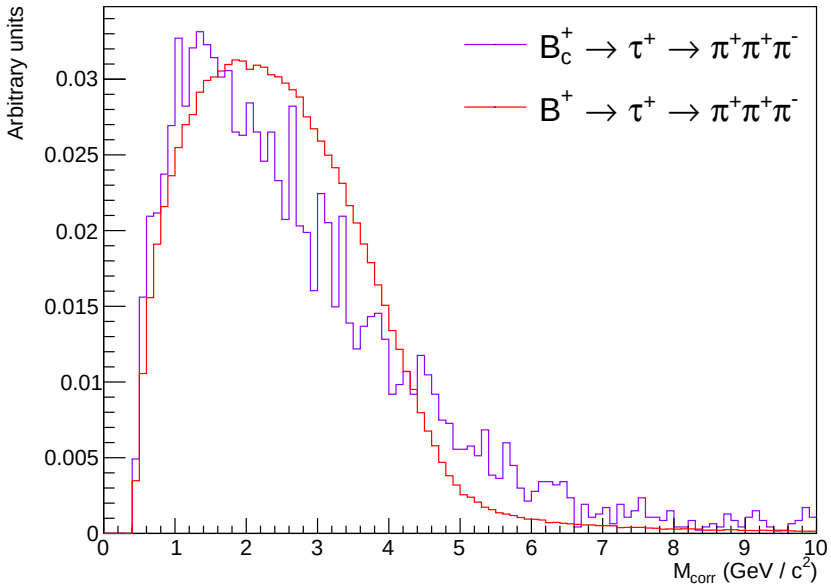

Figure 3.2: Normalized reconstructed invariant mass distributions of B^+ and B_c^+ decays. The B_c^+ distribution is composed of less events due to the low efficiency of B-Tracking for B_c^+-mesons

3.3 Simulation methods

Simulated decay events are an essential step to give insight in what a B-Tracking analysis could look like. What the characteristics are of events that leave a hit in the VELO, how many can be expected over the course of run 3 and other questions can be answered through simulation. However there are two options to consider: the full simulation package used in most LHCb analyses, or a much faster and simpler program called RapidSim[23]. The full software package is composed of several components including *PYTHIA*[24] to generate proton-proton collisions, *EvtGen*[25] for the resulting particle decays and *PHOTOS*[26] and *Geant4*[27] for the consequent radiation and detector response, respectively. The full suite configured for the LHCb collaboration is called *GAUSS* and provides great accuracy and detail. Important to note is that *GAUSS* provides a dataset composed of reconstructed objects, rather than just simulated particles. However, the 'true' characteristics of the original simulated objects are also available. RapidSim, on the other hand, uses a first-order approximation of the kinematic distributions from which to generate decay events, and does not simulate the detector response. In return, the generation process is many times faster, hence the name.

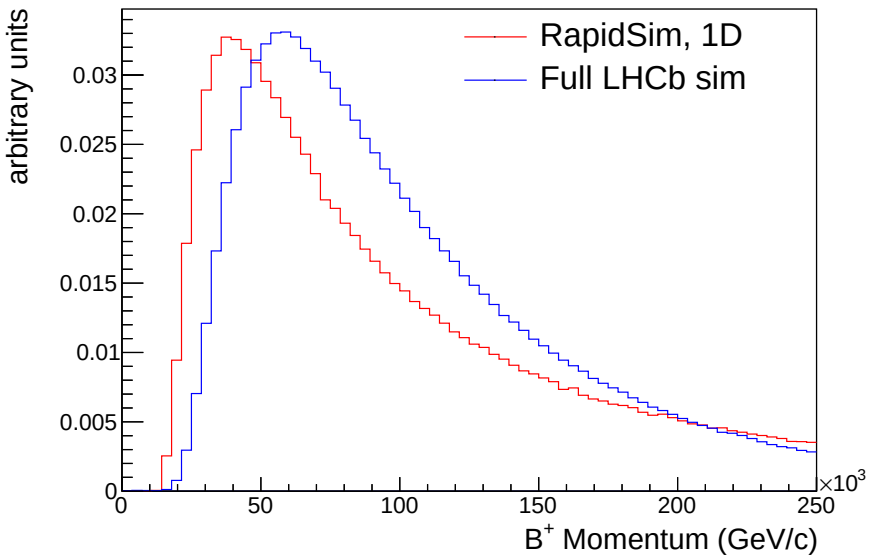

Figure 3.3: Normalized B^+ momentum distributions for RapidSim and the full LHCb simulation package, dubbed 'full sim'. A limited range is shown to highlight the difference.

Early on, differences were observed between simulated datasets in both kinematic distributions and resulting B-Tracking efficiencies. This is to be expected as they vary considerably with generating conditions and final state cuts. It is important however, to understand where the differences arise to justify the results obtained from simulation. A first evaluation of the two simulation methods would therefore be to compare the momentum distributions of B^+ mesons. The total momentum is representative for the efficiency as relativistic effects produce a higher probability to reach a first VELO sensor. This is discussed in more detail in section 5.1. For all comparisons in this section, simulated $B^+ \to J/\psi(\to \mu^+\mu^-) \to K^+$ decays were studied since such simulated data was readily available. The conclusions drawn should be applicable to $B^+ \to \nu_\tau \tau^+(\to \pi^+\pi^-\pi^+\overline{\nu}_\tau)$ decays because in B-Tracking, the primary interest is in the parent meson kinematics. B-Tracking efficiencies are entirely determined by the parent meson characteristics. A first momentum comparison is shown in figure 3.3. Clearly, the distributions differ significantly.

The discrepancy in momentum distributions may be the result of one or more differences in the following aspects of the simulation:

- **meson kinematic distributions**
  RapidSim uses FONLL to determine the transverse momentum and pseudorapid-

ity distributions of heavy mesons[28]. These are determined as an approximation of theoretical predictions of meson production. Additionally, events are taken from both distributions individually. However, pseudorapidity—a measure for the angle with respect to the beam axis—and transverse momentum are not correlated parameters in this process. LHCb Full simulation employs a more elaborate process to produce kinematic meson distributions.

- **decay event generation**
  Although the characteristics of the resulting decay products are not directly examined, they can indirectly influence the observed meson momentum distribution. This is the case because LHCb's full simulation inevitably applies some filter on the basis of these final state characteristics; at the reconstruction stage for example, events are only retained if some requirements are met such as the final state particles staying in the angular acceptance of the detector.

- **reconstruction**
  RapidSim provides a simple set of all events that have been generated. Full simulation data provides a dataset composed of reconstructed objects; tracks likely to have been from some particle, clusters of hits possibly originating from one particle. Therefore, the full simulation dataset has effectively been filtered on the reconstructability of events on the detector level. Additionally, the reconstruction efficiency is not constant over the parent momentum range.

To determine the causes responsible, several other datasets are considered. A RapidSim dataset generated from a two dimensional (pseudorapidity vs. transverse momentum) distribution, incorporating the correlation between the parameters. Secondly a Monte Carlo (MC) dataset is included. MC data is generated using *GAUSS* but contains information on the generator level; the detector response is not calculated, resembling the scope of RapidSim simulation. MC generation provides a 'reconstructability flag', i.e. a Boolean value indicating whether a certain particle would have generated a reconstructed object on the detector level. The value of the Boolean is provided by so called relation tables linking 'MC truth' data with reconstructed objects. Requiring reconstructability of all final state particles yields a third addition: a MC dataset with a 'reco-cut'. The resulting distributions are shown in figure 3.4. All additions are positioned between the two original distributions. Two-dimensional generation in RapidSim produces a small improvement. The MC set without a reconstructability cut is almost identical to RapidSim, indicating RapidSim generation is in principle correct. The major shift towards the full simulation distribution is observed when the MC set with reco-cut is included. Although the statistical uncertainties muddy a clear comparison, the distribution seems to be very close to that of the full simulation suite.

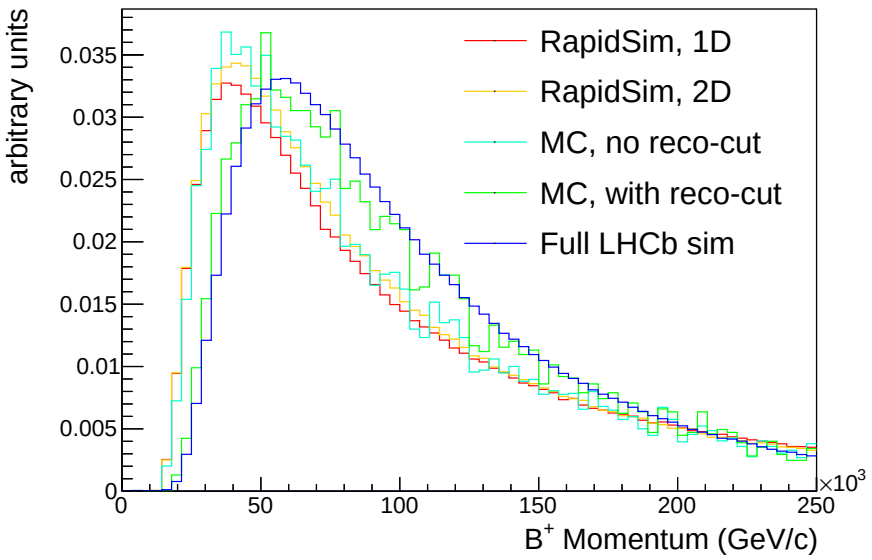

Figure 3.4: Normalized B^+ momentum distributions for 1D and 2D RapidSim datasets, Monte Carlo (MC) datasets with and without a cut on the final state reconstructability, and full sim. A limited range is shown to highlight the differences.

From these results it can be concluded that RapidSim datasets can responsibly be used throughout this feasibility study. The phase space generation is in line with that produced in full simulation. The main contrast is observed when taking into account the reconstruction of the event. Reconstruction only takes place given several requirements, which seem to be more easily satisfied for higher momentum events. Future results obtained while using RapidSim should therefore take into account that actual values obtained in data, e.g. B-Tracking yields, turn out different in practice. It is therefore important to compare such results with efficiencies obtained from data, which is one of the goals of chapter 6. On the other hand, the benefit of using RapidSim is considerable. The size of the simulated dataset is limited by CPU time and storage capacity. Given the very low efficiency of B-Tracking, fast simulation is essential to generate enough events that trigger the B-Tracking tool. Therefore, RapidSim is used for simulation throughout this study.

3.4 Results: efficiencies and yields

Once the simulation software is validated and background channels of interest have been established, some first estimates can be produced. Using the production cross-section of the 4 meson types, and taking the relevant branching ratios from the PDG, the results were obtained shown in table 3.1 [18, 29, 30]. The efficiencies have been determined by simulating a dataset of 10^7 decays for each channel in default LHCb geometric conditions. In practice, this comes down to the fact that the event is simulated in a direction that is in principle visible to the detector. No cuts were applied, as the production rates have been corrected for selection requirements, acceptance of the detector and so on. The obtained yields and efficiencies are therefore with respect to the total amount of produced mesons. In an analysis with a corresponding selection procedure, the efficiency of BTracking will turn out higher, but the absolute number of events of course lower.

The expected yields paint an optimistic picture. As 1 year of data-taking in run 3 will provide up to 10 fb^{-1} integrated luminosity, the *b*-mesons passing a VELO sensor will quickly reach numbers allowing for both a leptonic B^+ and a B_c^+ decay analysis. B-Tracking efficiencies are also determined for run 2 conditions with a less dense VELO station, to demonstrate that the potential of B-Tracking hinges on the LHCb upgrade. As the upgraded detector is hopefully completed soon, this is the appropriate time to prepare a charged B analysis with B-Tracking.

Another noteworthy observation is that *c*-mesons are produced in much larger numbers than their heavier counterparts. Given the comparable B-Tracking efficiencies for all meson types, the major contribution to VELO hits will be of background type meson decays. It is therefore of paramount importance to accurately separate signal events from the haystack that is B-Tracking *c*-meson hits, which is the subject of the next chapter.

Table 3.1: For signal- and background-type mesons, from top to bottom: total meson production rates per fb^{-1}, branching fractions for the studied decay channel, efficiencies under run 2 and run 3 conditions and the total expected signal decay events expected per fb^{-1} under run 2 and 3 conditions, with a B-Tracking hit requirement.

Meson	B^+	B_c^+	D^+	D_s^+
Production rate/fb^{-1}($\cdot 10^{-9}$)	87	0.6[1]	834	353
$\mathcal{B}(\to \tau \to \pi\pi\pi)(\cdot 10^4)$	0.159 ± 0.011	32.7 ± 2.3	1.75 ± 0.40	79.7 ± 3.4
η_{run2}	$5.0 \cdot 10^{-4}$	$1.7 \cdot 10^{-6}$	$1.6 \cdot 10^{-4}$	$6.6 \cdot 10^{-6}$
η_{run3}	$1.8 \cdot 10^{-3}$	$1.2 \cdot 10^{-5}$	$7.0 \cdot 10^{-4}$	$4.0 \cdot 10^{-5}$
B-Tracking yield (run2)/fb^{-1}	$(0.69 \pm 0.4) \cdot 10^3$	3.4 ± 0.3	$(2.33 \pm 0.91) \cdot 10^4$	$(1.84 \pm 0.08) \cdot 10^4$
B-Tracking yield (run3)/fb^{-1}	$(2.49 \pm 0.15) \cdot 10^3$	24 ± 2	$(1.02 \pm 0.40) \cdot 10^5$	$(1.12 \pm 0.05) \cdot 10^5$

Chapter 4

Signal Selection: *c*-Meson Background

The following chapter will present the feasibility of a charged b-meson analysis with respect to charmed background modes. The next chapter will deal with combinatorial background, but first the specific background modes discussed in chapter 3 will be tackled. To recap: the $B^+_{(c)} \rightarrow \nu_\tau \tau^+ (\rightarrow \pi^+\pi^-\pi^+\overline{\nu}_\tau)$ decay channels are considered signal. The background that will be studied here and separated from signal are the $D^+_{(s)} \rightarrow \nu_\tau \tau (\rightarrow \pi^+\pi^-\pi^+\overline{\nu_\tau})$ decay channels. In all cases, the charge conjugates of the decay channels are also implied. Variables that are presumably distributed differently for the signal and background channels, will be evaluated with Monte Carlo simulation using RapidSim [23]. Cuts on individual variables will not yield an effective background filter. Therefore the variables will be combined in a multivariate analysis—or MVA. The machine learning algorithm used in this analysis is scikit-learn: a readily available, open-source library for Python[31].

Generally speaking, a multivariate analysis is good at predicting values—in this case classifying data—by combining several pieces of information. The predictions are made on the basis of patterns in the data that might very well have been overlooked by the human researcher, or are too complex to stand out. As such, it is worth-wile to first filter the data based on the characteristics that have not slipped ones scrutiny. The resulting problem will then be a 'best first attempt'. Only then using a MVA to improve the analysis will cause the algorithm to focus its efforts on the data that have escaped prediction so far. In the context of particle physics, this amounts to filtering as much background as possible while keeping a considerable fraction of the signal. Using a MVA consequently, one will obtain the best resulting signal to background ratio.

First we will probe the variables available: elemental kinematic variables such as the (transverse) momentum of the final state particles and specific variables expected

to differ between signal and background. A short discussion of a multivariate analysis through machine learning will be followed by the analysis itself, showing the classifying power of BTracking information in filtering background from signal.

4.1 Observables of interest

A number of observables that can be included in the MVA are first discussed. As more variables are combined, a higher-dimensional fit has to be performed. Consequently, this requires more statistics and computing time to perform. If observables produce different distributions for signal and background events they possess differentiating power and are a meaningful addition to the analysis.

Meson momentum

The (transverse) momentum of the parent particle is an essential parameter. The momentum is approximated by taking the sum of the momenta of the reconstructible final state particles. In both simulation and data, the momentum is fundamental in determining other parameters, such as the opening angle and invariant mass. Therefore the information is always included in both in RapidSim datasets and in an actual LHCb data, regardless of the exact information that has been saved during data taking.

The momentum distributions in figure 4.1 show some differences between meson types. B_c^+ and D_s^+ mesons have a lifetime around 0.5 picoseconds, which is significantly less than that of B^+ and D^+ mesons. A higher Lorentz factor,

$$\gamma = \frac{1}{\sqrt{1 - v^2}} \tag{4.1}$$

where v is the speed in units of the speed of light, explains why the shorter-lived mesons favour higher momenta as seen in figure 4.2. The high-speed particles are affected by time dilation extending their lifetime, increasing the probability of hitting a VELO sensor. Given the variations in momentum distribution and the fact that information regarding the momentum is readily available, the observable is included in the MVA.

Meson transverse momentum

The transverse momentum of the parent particle shares the same traits as the total momentum, and is determined in the same manner. Also, the transverse momentum distributions show the same characteristics as the momentum distributions. This is no surprise, as the transverse momentum is a component of the total momentum. However, in terms of the probability of hitting a VELO sensor the similarity persists. As the VELO sensors

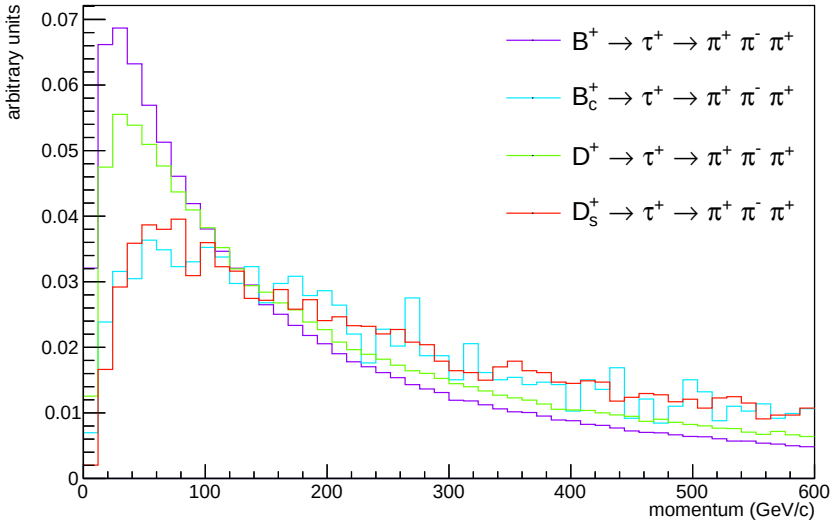

Figure 4.1: Normalized momentum distribution of signal and background events. All distributions are cut on passing at least one VELO sensor.

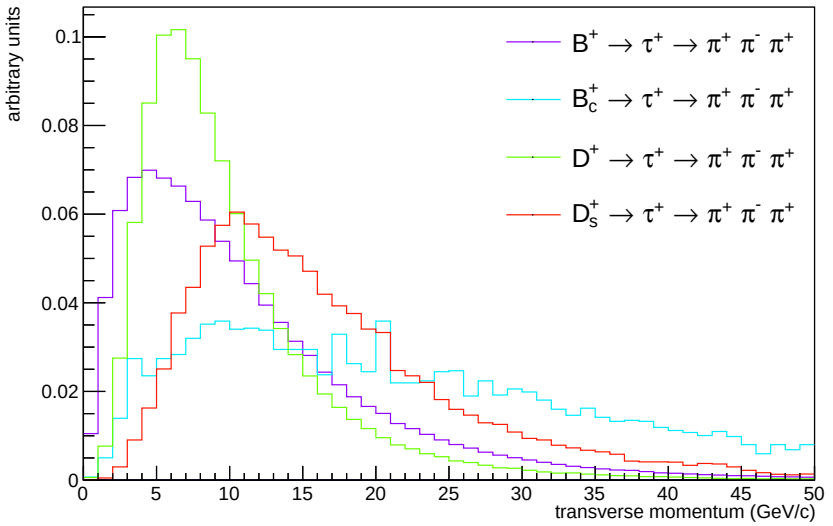

Figure 4.2: Normalized transverse momentum distribution of signal and background events. All distributions are cut on passing at least one VELO sensor.

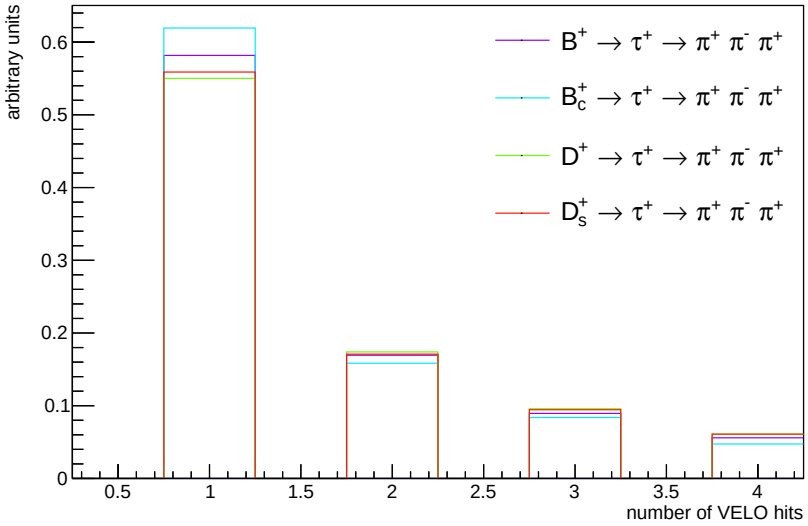

Figure 4.3: Normalized histogram for the number of VELO sensors passed for signal and background events.

will sit about 5 millimetres away from the beam axis for the upgraded detector used in run 3, mesons not only have to move sufficiently far along the beam axis to come across a sensor, but also a minimum distance away from the beam axis – in the transverse direction. This condition explains why shorter-lived mesons favour higher transverse momenta when a VELO hit is required. Additionally, heavy particle production cross-section are transverse momentum dependent. As such, the correlation would presumably be observed without a B-Tracking cut as well.

The other consideration for including the total momentum in the MVA is also applicable here. Transverse momentum information is readily available in a leptonic *b*-meson decay analysis, regardless of the exact fashion in which it is done. Therefore, the transverse momentum is also included in the MVA.

VELO hits

The analysis methodology proposed in this thesis is based on the hits left in the VELO sensors. As such, the number of VELO sensors hit before a meson decays is available and possibly informative of the meson type, given the different lifetimes and momentum distributions. Naturally, this information is only available when BTracking is applied. Figure 4.3 shows the variation to be modest. Therefore the fitting procedure described in the next section was performed with and without the number of VELO hits included as

a parameter. As the added parameter did not cause any speed or stability issues, it was included although the increase in performance is marginal.

Corrected invariant mass

In chapter 4, invariant mass was discussed to some extent. When all final state particles are detected, the rest mass of their parent particle can be determined through the energy momentum relation:

$$m_0 c^2 = \left(\frac{E}{c}\right)^2 - |\mathbf{p}|^2, \tag{4.2}$$

where $\mathbf{p}$ is the combined four-momentum of the final state particles, and E their combined energy[32]. As both energy and four-momentum are conserved in relativistic decays, the equation can be solved for the mass in any reference frame. The lowest possible energy in any reference frame equals the invariant mass, which is the rest mass of the parent particle.

In the case of the leptonic b-meson decays, the calculation is more complicated. At both vertices in the decay a neutrino escapes with an unknown fraction of the momentum that cannot be observed. The invariant mass can then be approximated by estimating the combined transverse momentum of the detected final state with respect to the flight direction of the meson. This transverse momentum is 'added' to the invariant mass calculation to account for the missing transverse momentum of the neutrino. The longitudinal neutrino momentum is lost. This yields the *corrected* invariant mass:

$$M_{corr} = \sqrt{M_{\pi\pi\pi}^2 + |p_\perp|^2} + |p_\perp| \tag{4.3}$$

where $M_{\pi\pi\pi}$ is the rest mass of the three final state pions and $|p_\perp|$ is the transverse momentum with respect to the meson flight direction of the final state particles.

The accuracy of the reconstructed mass is strongly dependent on the determination of the meson flight direction. Normally, the meson direction is taken to be from the primary vertex (PV) to the secondary vertex (SV). As the intermediate τ presumably has a flight distance of the same order as the meson, the PV-SV direction can diverge substantially from the actual meson direction. The BTracking tool aims to determine charged meson directions directly and will therefore enhance corrected mass calculations measurably. Figure 4.4 and 4.5 show corrected mass distributions for signal and background events with and without using BTracking meson flight direction, respectively.

Two observations are worth mentioning. First and foremost, the corrected mass distributions contain information of the type of meson – the two missing neutrino's notwithstanding. Thus, it is included in the MVA. Secondly, the effect of using BTracking information in determining the corrected mass is apparent. Comparing figure 4.4 with figure 4.5,

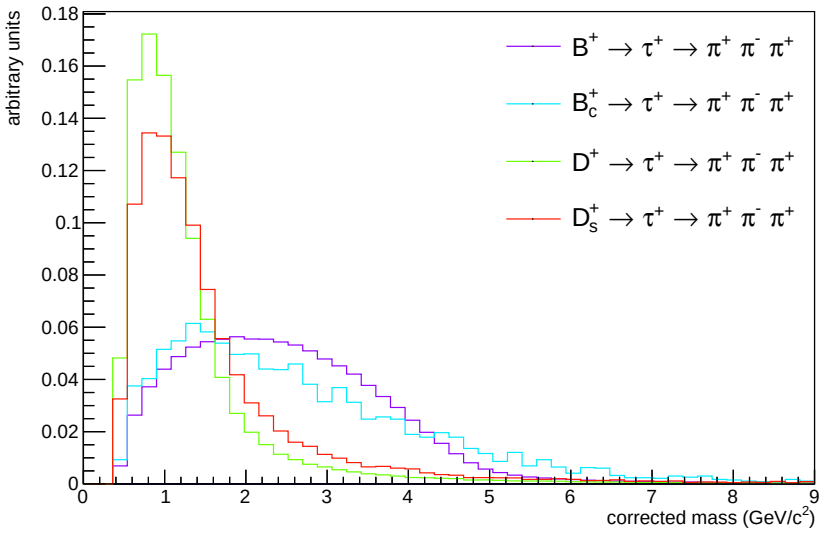

Figure 4.4: Normalized corrected invariant mass distributions for signal and background events. Correction is based on the PV–SV direction. All distributions are cut on passing at least one VELO sensor.

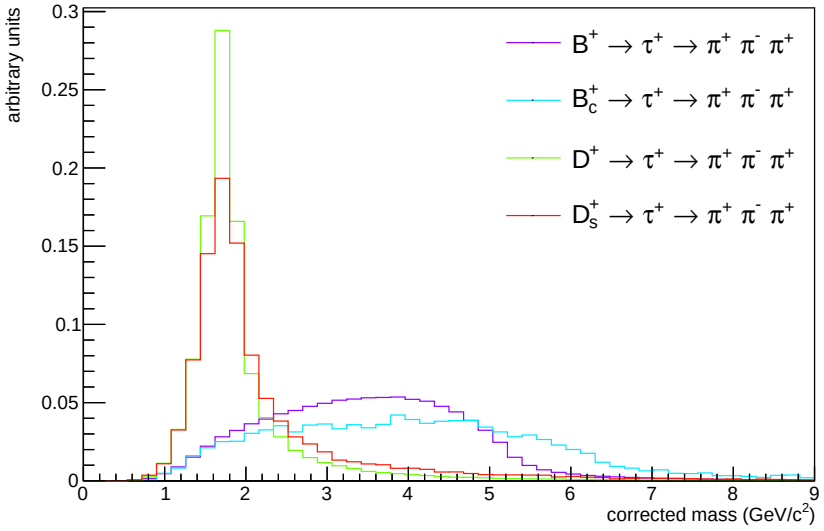

Figure 4.5: Normalized corrected invariant mass distributions for signal and background events. Correction is based on the BTracking meson direction. All distributions are cut on passing at least one VELO sensor.

the improved distributions peak stronger and much closer to the actual rest mass of the *c*-mesons – just under 2 GeV/c^2. Also, the signal to background ratio is more favourable as the distributions for the *b*-mesons shift closer to their rest masses of 5 to 6 GeV/c^2.

Opening angle

The final observable to be discussed is significant due to the same underlying principle. The opening angle is the angle between the daughters in a two-particle decay. In the context of a $B^+_{(c)} \rightarrow \nu_\tau \tau^+ (\rightarrow \pi^+\pi^-\pi^+\overline{\nu}_\tau)$ decay, this relates to the angle between the τ and the (anti-)neutrino coming from the first decay vertex. The opening angle θ can be inferred from the following formula for the invariant mass of the parent particle:

$$M_{inv} = \sqrt{m_\tau^2 + m_{\nu_\tau}^2 - 2p_\tau p_{\nu_\tau} cos\theta + 2\sqrt{m_\tau^2 + p_\tau^2}\sqrt{m_{\nu_\tau}^2 + p_{\nu_\tau}^2}}. \tag{4.4}$$

For a short derivation of the equation, see chapter six of [33]. For a given meson momentum, the rest mass of the meson determines the opening angle; a higher invariant mass produces a larger opening angle. The opening angle at the meson decay vertex is potentially telling of the parents' rest mass. Two issues arise when determining the opening angle, however. The neutrino's flight direction is not accessible. Instead the angle between the τ and the meson's flight direction is taken. The problem is aggravated because the flight direction of the τ is not accessible either. Summing the momenta of the final state pions produces a best estimate. Therefore, whenever 'opening angle' is used, what is really meant is the angle between the meson flight direction and the pion triplet flight direction.

Disregarding the obstacles just discussed, the opening angle might yet prove an interesting observable in signal selection. Figure 4.6 and 4.7 show distributions of the opening angle without and with BTracking information included, respectively. The latter shows promising differences for the heavier meson types. Hence, the opening angle is included in the MVA.

4.2 Multivariate analysis

The term 'multivariate analysis' has been used imprecisely in this chapter so far. All this declares is that several variables together – the ones just discussed – are used for analysis. In this section the method will be described explicitly, including the pitfalls of using machine learning as a tool for classification. The goal is to create a *test statistic* that expresses whether an event is likely to be signal or background, in a relative sense. Selecting signal above a chosen value for the test statistic will then yield a dataset with the desired trade-off between signal to background ratio and efficiency.

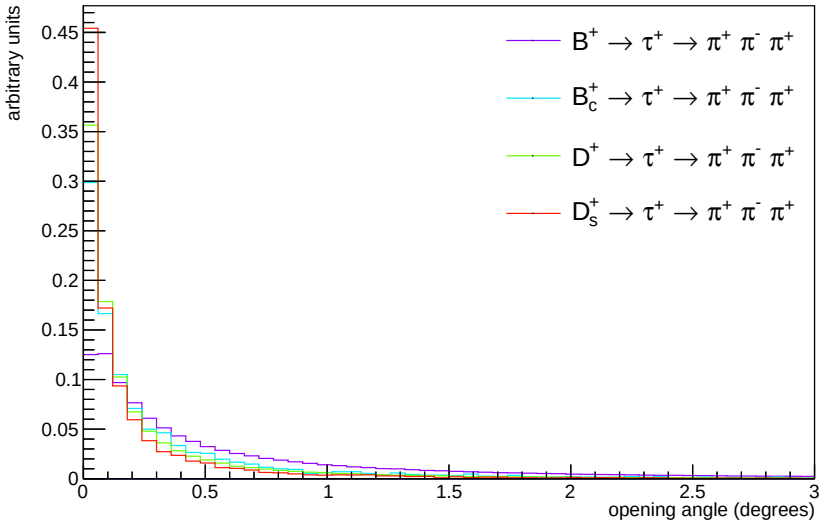

Figure 4.6: Normalized 'opening angle' distributions for signal and background events. The angle is determined with the normal meson direction information: PV–SV. All distributions are cut on passing at least one VELO sensor.

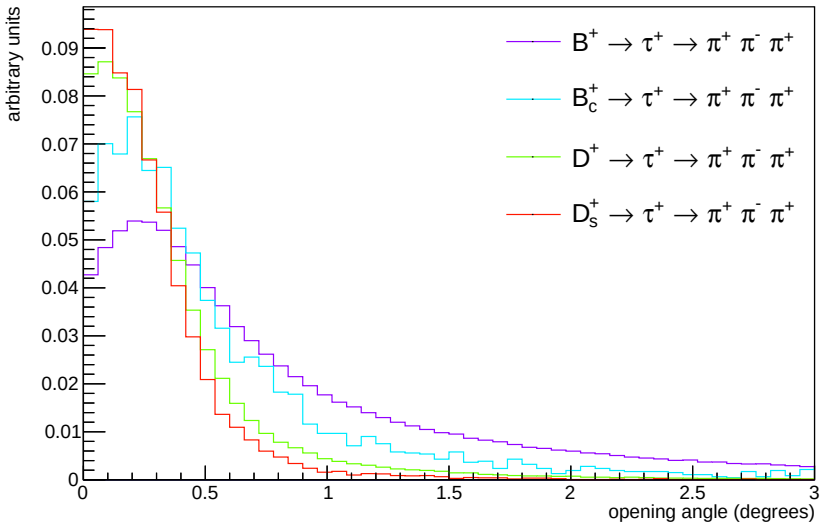

Figure 4.7: Normalized 'opening angle' distributions for signal and background events. The angle is determined with the BTracking meson direction information. All distributions are cut on passing at least one VELO sensor.

After the stage has been set, the results are presented for a MVA using BTracking information, and for one using the standard information available for the meson flight direction. Finally, the classification is shown to be largely based on two variables: the corrected mass and the opening angle. These variables are investigated more closely, in order to conclude that background can be filtered sufficiently from signal given their expected relative yields in the upgraded LHCb detector.

4.2.1 Machine learning classification using scikit-learn

For the multivariate analysis presented here a Gradient Boosting Classifier (GBC) algorithm is used. The classifying technique is part of the scikit-learn module for Python[31]. The Gradient Boosting classification aims to minimize the loss-function – the number of faslsely classified events – using a number of decision trees. The boosting process is iterative as every new tree is created based on how well the previous tree has performed. For the GBC used here, many 'weak learners' – boosted decision trees (BDTs) – with a weight proportional to the rate of correctly classified events are trained. The weighted sum of all the decision trees then yields a test statistic representing the prediction that a newly presented data point is of a particular class.

In the context of signal selection, this is a binary classification problem. Simulated signal and background events are flagged given their nature: signal events fall in one category, while background events fall in the other. The `n-estimators` of BDTs are then trained on a subset, the 'train-set' of the dataset – typically half. The performance of the dataset is determined by calculating the predictions of the GBC of the remaining subset of events that were not used in training, the 'test-set'. The performance is measured by the false positive and true positive rates, (FPR and TPR). The FPR and TPR are plotted against each other to produce a curve of the receiver operating characteristic, the ROC curve. The curve displays what FPR can be expected for a certain TPR, i.e. how many background events are falsely classified as signal for a certain signal selection efficiency. The 'area under curve' (AUC) represents the success of the classification, with an AUC of 1 being a perfect score.

One of the main concerns in running a machine learning algorithm is over-training. Over-training can occur when either the complexity or the training time of the model is too great. This can result in a model that is fit on the particularities—statistical fluctuations lacking a physical cause—of the train-set very well, but because of that fails to generalize to other datasets of the same nature, but with different fluctuations[35]. Figure 4.8 illustrates the problem.

Throughout the analysis here, the following choices have been made for the configuration of the GBC in accord with the findings in [36]. `n-estimatiors = 100`: 100 BDTS are used in training. `tol = 1e-4`: the training is terminated when a relative im-

provement of less than one in ten thousand is detected. `max depth = 3`: the maximum depth of the decision trees is set to three. The division between the training and testing sets is 50/50. These are all default values as there is little to be gained in departing from the default, and they are a robust choice with respect to over-training.

4.2.2 Results

Gradient boosting classifiers have been trained with the observables and configuration discussed in the previous sections. A dataset was simulated with RapidSim, containing all 4 decay channels in quantities proportional to the BTracking efficiency and cross-section of each meson type. The dataset is composed out of approximately 1 million events. The GBCs are trained to distinguish signal from background, in order to improve the signal to background ratio of the intended analysis. One classifier is trained on a dataset with variables determined without BTracking information, another is trained on a dataset with variables including BTracking information. Both datasets require at least one B-Tracking hit, however. BTracking information adds improved values for corrected mass and the opening angle, and naturally the number of VELO hits. Both classifiers include the same momentum and transverse momentum. The results are shown in 4.9.

The results make a convincing case for the use of BTracking information. An improvement is expected as more relevant information generally leads to better classification, but two observations are of particular import here. First of all, a background rejection rate of 99.9% can be achieved while retaining half of the signal events. Classifying without

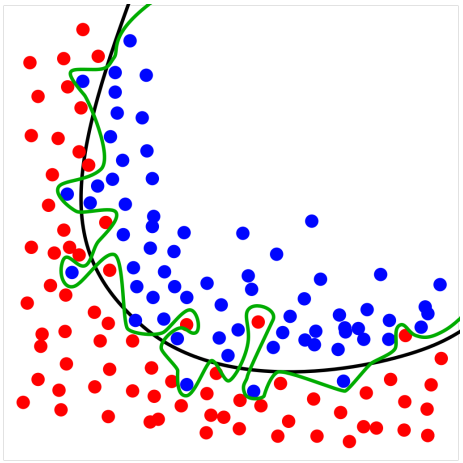

Figure 4.8: Illustration of over-training in binary classification. The black line represents an adequate model separating the different classes of dots. The green line represents an over-trained model that fits this particular data perfectly, but does not generalize well to other data. Figure from [34]

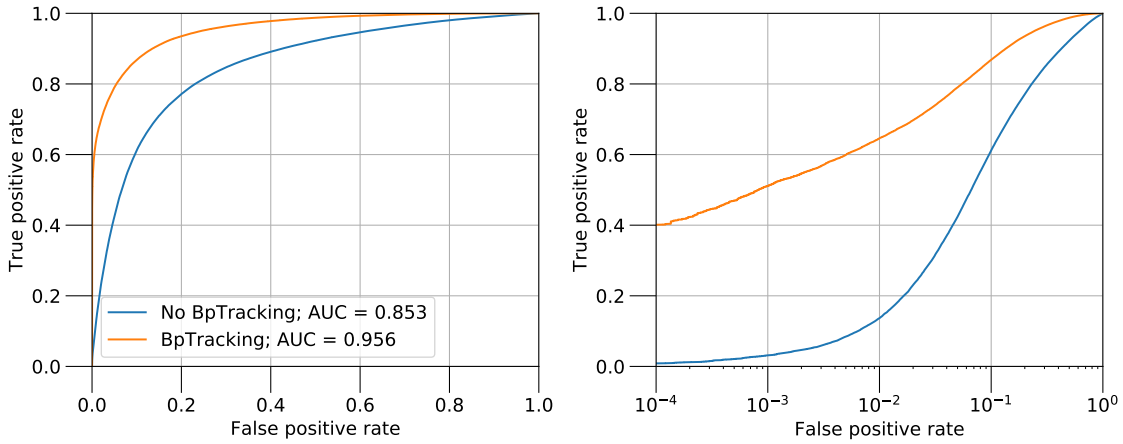

Figure 4.9: ROC curves of classifiers with and without using BTracking information. The left figure shows the curve on a linear scale, the right plot on a logarithmic scale to display the area of interest around an FPR of 10^{-3}. Variables used for 'No BTracking': P, PT, opening angle, M_{corr}. Variables used for 'BTracking': P, PT, *opening angle*, M_{corr}, *number of VELO hits*. Italic variables are determined using BTracking.

BTracking information retains less than 5% of the signal for the same background rejection rate. This shows that a multivariate analysis alone is able to suppress background sufficiently to obtain signal to background ratios for a feasible analysis.

Secondly, the ROC curve indicates that a significant fraction of the signal can be correctly classified seemingly without including any false positives. Although the resolution is limited to a FPR of around 10^{-4} because of the size of the dataset, this 'pure' signal is worth investigating further. If a certain volume of the parameter space is lacking any background, it is sensible to find out what volume that is.

From the start, the opening angle and corrected mass have shown to be the most differentiating observables. As such, it is understandable that the same variables delineate the parameter space of interest. Figure 4.10 and 4.11 show the distributions of the corrected mass and opening angle respectively. The full dataset and signal and background events are plotted as well as 'pure' signal. Pure signal is obtained when the dataset is cut on the threshold value of the trained classifier for which all background has been filtered. Both histograms show a lower cut-off for the pure signal distribution. As these individual cut-offs do not explain a background-free subset of events, the two-dimensional parameter space is plotted as well.

Figure 4.12 and 4.13 show two-dimensional histograms of the opening angle plotted against the corrected mass for signal and background, respectively. The figures clearly

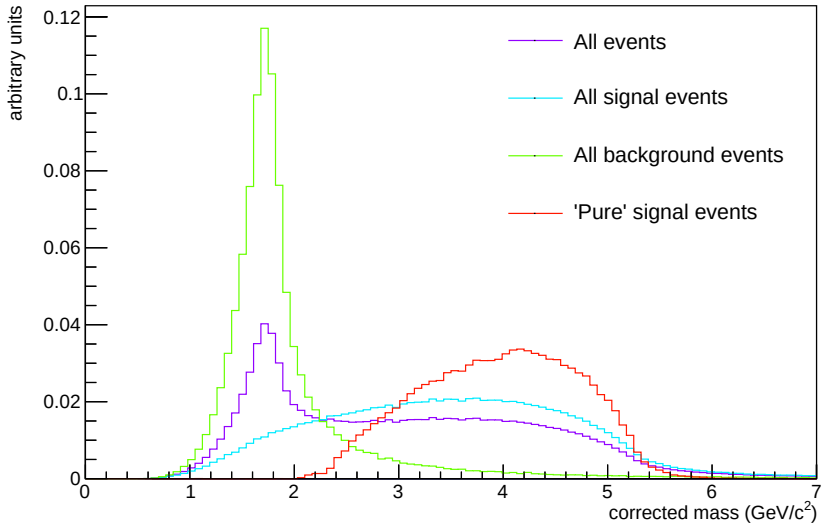

Figure 4.10: Normalized corrected invariant mass distributions of all data, signal only, background only and pure signal. All distributions are cut on passing at least one VELO sensor. A lower cut-off is observed at 2 GeV/c^2 for pure signal.

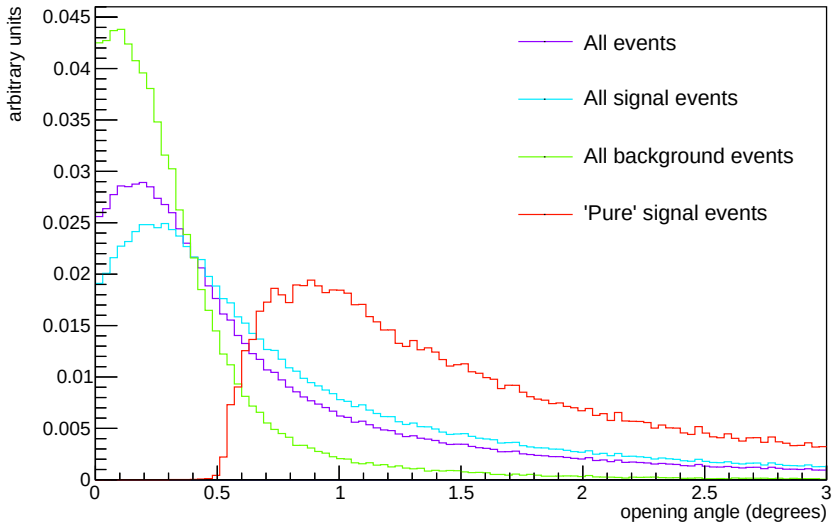

Figure 4.11: Normalized opening angle distributions of all data, signal only, background only and pure signal. All distributions are cut on passing at least one VELO sensor. A lower cut-off is observed at 0.5 degrees for pure signal.

indicate on what characteristic the MVA has selected the subset of pure signal: both cut-offs combined define a section of the parameter space that contains a significant fraction of signal events, but for which the background distribution is almost empty.

First of all, the observation that two simple kinematic cuts produce a selection that suppresses *c*-meson background entirely – given the sample size of about 1 million events – in addition to the fact that a satisfactory false positive rate can be attained while keeping as much as half of the signal is promising. However, some remarks are in order. All data that has been used in this chapter was simulated using RapidSim[23]. As we have seen, the differences between simulation methods are not negligible. When the detector response is considered in full simulation, reconstructability of the final state might for example paint a less conclusive picture of the proposed signal selection methodology. Also, as mentioned in chapter 3, the background decay channels studied here are an educated guess at the most numerous and troublesome type of background. This background can be effectively suppressed, but by no means the conclusion should be drawn that a search for leptonic *b*-meson decays is unhindered by background. The combined effects of combinatorics, misreconstructions and noise will most likely produce signal candidates but can only be studied in real data.

A final note goes back to the statement at the beginning of this chapter. The intended use of a MVA is to recognize the patterns in a dataset that the human eye has missed in order to improve upon the first classifying attempt. This has not been the approach here, as the two dimensional cut proposed here has come to light through the use of the MVA. In line with our own advise, the best classification is made by first cutting on the corrected mass and opening angle, and subsequently running a MVA algorithm to exploit the other characteristics of the dataset. This would be a prudent next step in determining a signal selection procedure.

In short, a charged B-Tracking analysis has been shown to be feasible in terms of charmed background modes, despite the low efficiency of the BTracking tool. What is presumed to be the most abundant type of background can convincingly be suppressed and the supplemental information gained from the BTracking tool is crucial in that process. The MVA can be improved and further study is required to determine the signal selection completely. What has been shown here is the viability of a direct *b*-meson measurement approach with respect to $D^+_{(s)}$ background.

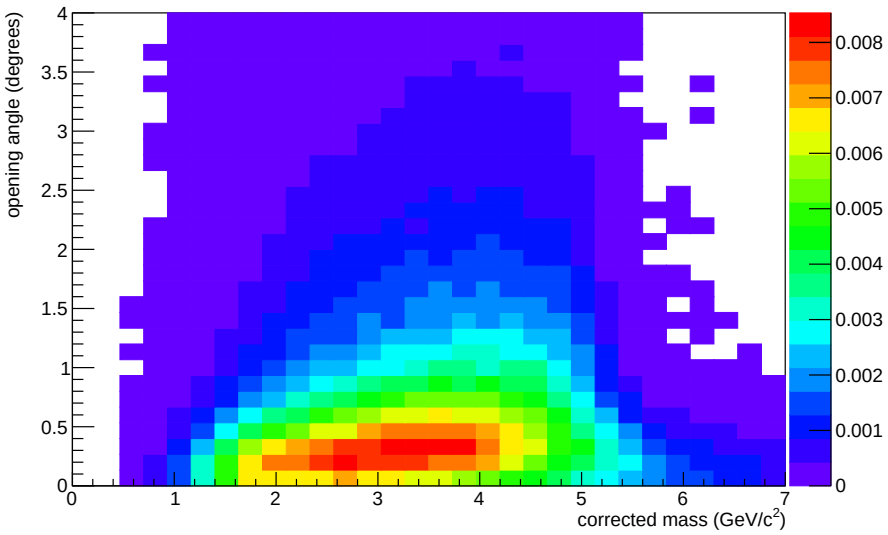

Figure 4.12: Normalized two-dimensional distributions of the opening angle vs. the corrected invariant mass of signal events.

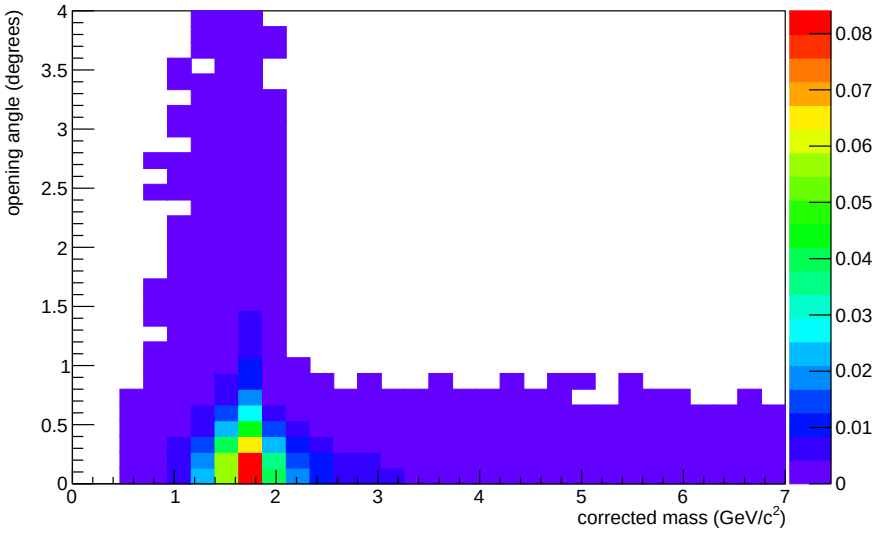

Figure 4.13: Normalized two-dimensional distributions of the opening angle vs. the corrected invariant mass of background events.

Chapter 5

Signal Selection: Combinatorial Background

In this chapter the use of the BTracking tool will be studied in practice. The BTracking tool is applied to real LHCb data from 2018. The resulting dataset is the first example of real data with BTracking information. The analysis of this data will serve two purposes: to show that BTracking can correctly identify charged meson hits in the VELO, so that the data can serve as a check for our preliminary estimates. The dataset will affirm an efficiency in line with expectations.

Additionally, the effect of requiring at least one VELO hit on combinatorial background can be determined. Combinatorial background is a random combination of final state particles in the detector coming from separate decays that together pass the background filter. Combinatorial background is inevitable in any analysis and has to be dealt with separately from specific backgrounds. Requiring a VELO hit has a significant impact on combinatorial background numbers. In the dataset, 434 ± 32 events triggered a VELO hit while not a single of those can be attributed to combinatorial background. The results are obtained by finding the signature of the signal and the background separately over the invariant mass distribution of the whole dataset. These signatures are then fit to the invariant mass distribution for data for which one or more VELO hits is required. Converting these signatures to a subset of the data is assumes the B-Tracking cut to be uncorrelated with the invariant mass. The result is a yield for the signal and background, the last of which is 0. These findings allow us to put an upper limit on the expected combinatorial background in the invariant mass region of the B^+, between 4850 and 5750 MeV/c^2

This chapter will briefly cover the software package that is used for the fitting, RooFit. Then, an example of an invariant mass fit of the $B^+ \rightarrow J/\psi(\rightarrow \mu^+\mu^-) \rightarrow K^+$ decay is treated. The decay will function as a control channel for the $B^+ \rightarrow \nu_\tau\tau^+(\rightarrow$

$\pi^+\pi^-\pi^+\overline{\nu}_\tau$) decay, as it is well understood and ample data is available. The fit provides the information to calculate the sWeights of the mass distribution. Although sWeights are not used in further analysis, they can also be used to retrieve variable distributions that are uncorrelated to the fitting variable. The example is a small showcase of the potential of using sWeights. Additionally, it will serve to understand how the method can be applied to separate the mixture of B^+ and B_c^+ mesons and project out variable distributions of either meson. After the example fit, the same method is applied to real data, resulting in an upper limit on combinatorial background in a BTracking analysis.

5.1 Invariant Mass Fitting using RooFit: an Example

RooFit is used with the MINUIT package to fit the invariant mass [37][38]. MINUIT performs a maximum likelihood fit, i.e. a probability density function (PDF) is created that produces the highest likelihood that the given data points have been produced by the PDF. The probability density functions are constructed according to input parameters. RooFit supports many different predefined functions that can be used out of the box including Gaussian and exponential functions as well as more particular functions such as the Crystal Ball and ARGUS background.

The following example shows the invariant mass maximum likelihood fit of data of the $B^+ \to J/\psi(\to \mu^+\mu^-) \to K^+$ decay channel. The dataset is the result of run 1 data taking in 2011 and amounts to around 0.5 fb^{-1}. The data has originally been used as a calibration channel, and has passed corresponding trigger and selection requirements, all of which are based solely on the final state particles. Additionally, a `Kp_PIDK>5` cut is made to remove $B^+ \to J/\psi(\to \mu^+\mu^-) \to \pi^+$ partially reconstructed background present in the dataset. `Kp_PIDK` is a measure for the likelihood of the candidate kaon to be a kaon, based on data from the ring imaging Cherenkov subdetectors. First the invariant mass data is fitted with two separate PDFs for the signal. For the combinatorial background an exponential PDF is used. Allowing RooFit to adjust the parameters of the PDFs within a given range gives a maximum likelihood fit. The fit produces a yield for the signal and background.

Figure 5.1 shows the combined fit of the signal and background probability functions. The lower bar shows the 'pulls' in each bin; the discrepancy between the value of the total PDF and the number of events in a bin, in units of the error. The signal PDF is composed of 3 separate parts. A Gaussian function at its peak, with two tails at the higher- and lower-end. The tails are modeled by a Crystal Ball power-law, named after an old experiment at the Stanford Linear Accelerator Center (SLAC)[39]:

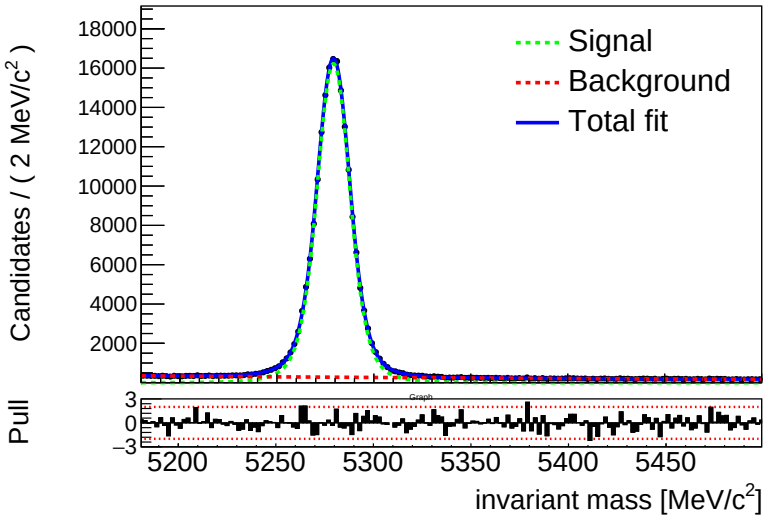

Figure 5.1: Fit over the invariant mass of the example dataset. The dashed lines show the signal and background components. The lower bar shows the pulls.

$$\text{CB}\,(m, \overline{m}, \sigma, \alpha, n) \propto \left(\frac{n}{|\alpha|}\right)^{n} \cdot \exp\left(-\frac{|\alpha|^2}{2}\right) \cdot \left(\frac{n}{|\alpha|} - |\alpha| - \frac{m-\overline{m}}{\sigma}\right)^{-n}, \tag{5.1}$$

where $\overline{m}$ and σ are the mean and the standard deviation of the Gaussian distribution. α is the location of the threshold where the Gaussian transitions into the tail, in units of σ. The exponential n controls the slope of the tail. The Crystal Ball distributions are necessary to accurately model the ends of the signal distribution. The invariant mass resolution is the result of the uncertainties of several variables such as final state momenta and directions, as well as possible final state radiation that together produce unsymmetrical, smeared tails.

All combined, the total PDF is parameterized by 9 independent parameters: four for the thresholds and slopes of the Crystal Balls, two for the Gaussian and one for the exponential background. Finally, two parameters represent the signal and background yield. The yields found for this dataset are:

$$\begin{aligned} N_s &= 186,808 \quad \pm 484, \\ N_b &= 39,774 \quad \pm 296. \end{aligned}$$

All results presented in this chapter are given with a 1σ error, i.e. a 68% confidence level, unless stated otherwise. It is important to note that the shapes of the signal and background components are essential information for the fitting procedure and in determining their respective yields. A common saying in the context of statistics is that given enough parameters, one can fit any model to any set of data-points. The a priori knowledge of the nature of the components is the only constraint on the otherwise great freedom 9 parameters provide.

The relative magnitude of the signal and background PDFs in each bin permit the determination of the sWeight of each bin. sWeights are chosen such that bins with a higher background PDF value, i.e. mostly background candidates, are given a negative weight and bins with a majority of signal candidates a positive weight. The weights are proportional to the signal to background ratio. Finally the weights are normalized such that the mean contribution of signal events is the signal yield found in the fit, while the contribution of background averages zero, as the contributions in bins with a positive weight is cancelled by bins with a negative weight. Therefore, using these sWeights effectively projects out the signal component of the data. sWeigths can also be calculated to project out the background component, such that the signal contribution averages to zero but the mean of the background contribution is the background yield. Both sWeight functions are plotted in figure 5.2, although typically only the sWeigths for the signal projection are used.

The weighted data can now be used to study the characteristics of the signal component. As the weighting is dependent on the invariant mass, the characteristics that can be correctly reconstructed must be independent of the invariant mass. If the characteristic is correlated with the invariant mass, negative contributions might not be cancelled out by positive contributions in all bins, possibly yielding a histogram with negative values, clearly indicating incorrect results. The lifetime of the B^+ meson is an example of an uncorrelated variable. The lifetime should therefore reveal different distributions for the signal and background components consistent with B^+ meson decays and combinatorial background, respectively.

Figure 5.3 shows the proper lifetime distributions of the signal and background projections. The signal distribution shows a lifetime of around 1.5 ps, consistent with the 1.638 ps reported by the PDG[18]. The background distribution does not show the exponential shape expected from the decay of a single type of particle. Both observations indicate that the weighting has been successful, as the signal appears to be composed of B^+ mesons, while the combinatorial background is made up of a combination of hits without a consistent lifetime altogether.

The example has illustrated how this specific reweighing enables the determination of the lifetime of our signal, while we only have access to a dataset containing a

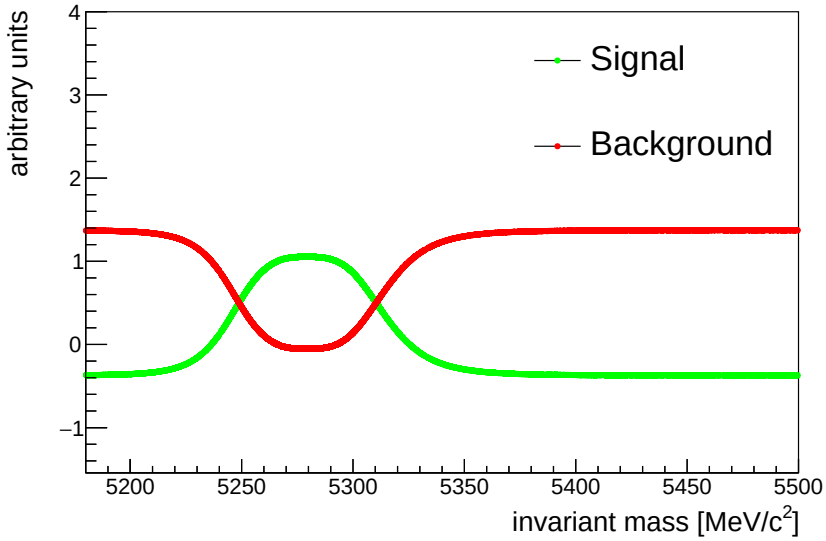

Figure 5.2: Plot of the sWeight values versus the invariant mass. sWeights for both the signal and background components are shown in green and red, respectively.

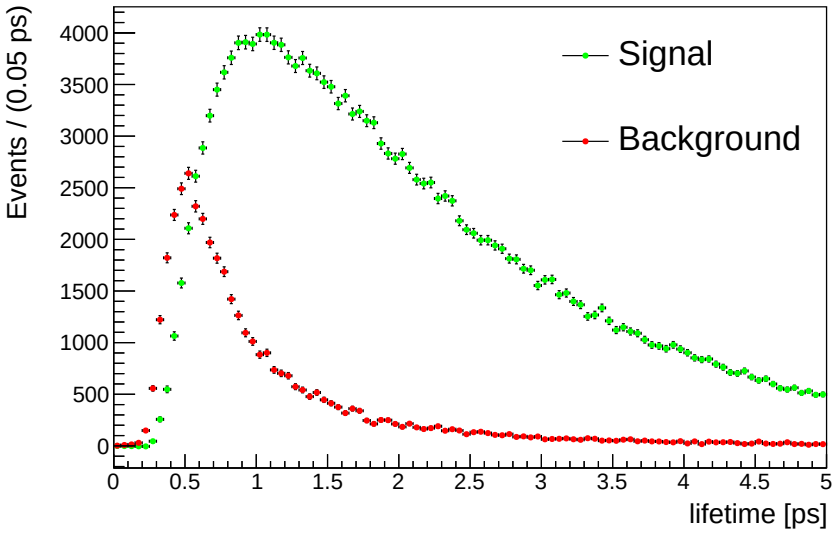

Figure 5.3: Distribution of B^+ meson candidate lifetimes for the signal and background projections of the dataset. The signal distribution is consistent with the B^+ lifetime, while the background is not consistent with a single lifetime.

mixture of signal and background. In the context of a B-Tracking analysis, we have up until this point always considered both B^+ and B_c^+ mesons as signal. Although their rest masses are different, we have seen in the previous chapter that a differentiation by their reconstructed invariant mass is hardly possible as the missing neutrinos remove the information required for a usable invariant mass resolution. However, using their lifetimes would paint a much clearer picture. The PDG reports the B_c^+ lifetime to be 0.51 ps which is less than a third of the B^+ lifetime. Fitting over the lifetime with the known shapes of an exponential decay as probability density functions would provide a yield for both meson types separately—just as we have seen for the invariant mass. The yields can then be translated into a relative branching fraction, assuming the relative efficiencies are worked out in more detail. Fitting over the lifetime would also allow for calculating the sWeights. The weights can project out any other unrelated variables of the two decay types, such as the B^+ momentum distribution. Comparing the data with simulation for the control channel, provides a measure for how simulation corresponds to data in terms of variables that are relevant to B-Tracking, for example.

5.2 Results

In the second part of the chapter, we will get into a real dataset that has been reconstructed from raw LHCb data with BTracking applied. The data is from 2018 as part of run 2 of data taking. The fitting procedure laid out in the last section is also applied here, albeit in a more complex form. The fit fixes the necessary parameters in order to transfer parts of the fit to a subset of the data, namely the events that triggered BTracking, i.e. the set with cut: `Bp_BpTracking_nHits>0`. Under the assumption that the BTracking cut does not significantly alter the shapes of the components of the signal distribution, they can be used to reevaluate the signal and background yield. The number of observed background candidates is statistically zero, resulting in an upper limit on the combinatorial background expected for this dataset when a BTracking trigger is required.

The data is selected for the same calibration channel as was used in the last section. The selection is based on final-state characteristics only. The dataset contains signal events peaked around the B^+ invariant mass, as well as partially reconstructed events that have produced the same final state. These partially reconstructed B^+ decays have produced one or two additional pions, yielding an invariant mass at least one or two pion masses lower than the B^+ mass. These contributions are modelled separately by an ARGUS background distribution, also named after an old collaboration [40]. Although commonly referred to as ARGUS 'background', in our case they represent part of the signal; we are fitting the number of correctly identified b-mesons by the BTracking tool. Whether this turns out to be a partially reconstructed event has no bearing on the success

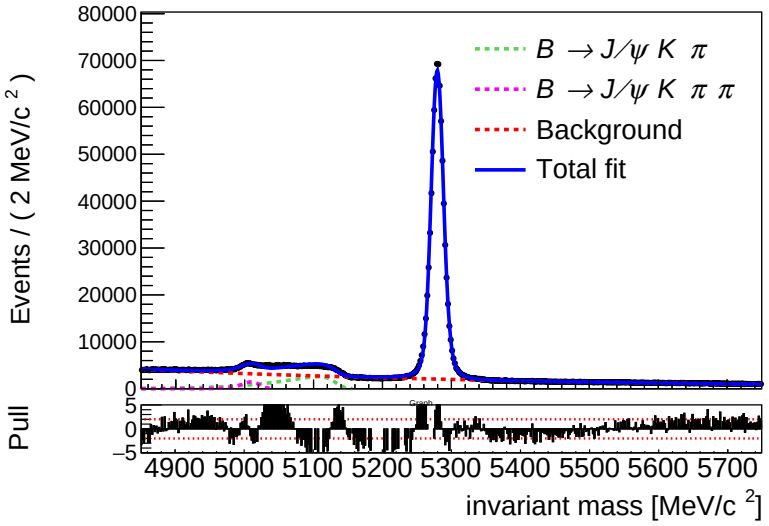

Figure 5.4: Invariant mass fit over the complete dataset. The signal component including the tails is not included for clarity.

of the BTracking tool in identifying and reconstructing a b-meson. However, some of the partially reconstructed candidates are presumably originating from a neutral b-meson, i.e. a $B^0 \to J/\psi K^+\pi^-$ decay. As neutral particles are not detected by the VELO, their decays should not count towards a higher B-Tracking efficiency. To be on the safe side, results will not include partially reconstructed events in the signal yield calculations.

The ARGUS distribution is modelled by the following formula:

$$\text{Argus}(m, m_0, c) \propto m \cdot \left[1 - \left(\frac{m}{m_0}\right)^2\right] \cdot \exp\left[c \cdot \left(1 - \left(\frac{m}{m_0}\right)^2\right)\right]. \tag{5.2}$$

m is the invariant mass variable over which the distribution runs, m_0 is the upper threshold value at which the distribution starts, determined by the rest mass of the meson minus the missing rest mass, i.e. $m_B - n \cdot m_\pi$ for n missing pions. c controls the shape of the distribution, with negative values forcing the peak near m_0 and positive values nudging the peak towards zero.

Figure 5.4 shows the fit of a probability density function composed of 4 parts. An exponential background just like we have seen in the example, a Gaussian with two Crystal Ball tails for the main signal peak and two ARGUS distributions, with m_0's appropriate for one and two missing pions. The Gaussian component is not plotted to avoid cluttering the plot. Although the pulls displayed in the lower bar show some improvement of the fit is possible, it is a sufficient fit for the precision at hand; the yields provide an estimate of

the minimum signal to background ratio improvement. Would a branching fraction have been calculated from the fit, a more precise determination of the signal yield is required. The following signal – including the ARGUS distributions – and background yields have been determined:

$$\begin{aligned} N_s &= 957,362 \quad \pm 1,406\,\text{(stat.)}, \\ N_b &= 970,833 \quad \pm 1,410\,\text{(stat.)}. \end{aligned}$$

The next step is to use the information from this first invariant mass fit in fitting the subset of data with `Bp_BpTracking_nHits>0`. The subset consists of 434 candidates. The parameters controlling the shape of the ARGUS distributions and the Crystal Ball tails are taken as constants in the invariant mass fit of the subset. The parameters of the Gaussian peak remain free as a wider signal peak is expected. The last chapter demonstrated that requiring a B-Tracking hit suppresses low momentum candidates, and the invariant mass resolution is inversely proportional to the candidate momentum. The background is left unfixed because much of the combinatorial background is expected to be cut away. The relative magnitudes of the components are not fixed either, as requiring a VELO hit is not expected to impact the efficiency of all components equally. The second fit is performed under the assumption that all components that are fixed do not change in shape under a VELO hit cut, but only in size. This assumption is correct only to some degree, but valid for the precision at hand.

Figure 5.5 shows the invariant mass fit over the subset of the data. The contributions of the partially reconstructed events left of the main signal peak have become smaller and the exponential background present in the original data has vanished and is therefore not plotted. Indeed, the yields found for the subset are:

$$\begin{aligned} N_s &= 434 \quad \pm 32\,\text{(stat.)}, \\ N_b &= 0 \quad \pm 1\,\text{(stat.)}. \end{aligned}$$

These results are in line with expected BTracking efficiencies studied in chapter 3, displayed in table 5.1. The B^+ reconstruction efficiency was found to be over half the efficiency in simulation. A dataset of 10 million events was simulated in RapidSim, mimicking the effects of selection requirements of the data that has been fit here. The cuts are shown in table 5.2. This left a little over 6 million events. The gap between the simulated and real efficiencies is explained by their origins: in RapidSim simulation, the efficiency is determined by studying the fraction of b-mesons that makes it through one VELO sensor. In the current dataset, the efficiency is the result of the number of fully or partially reconstructed events that pass one VELO. Therefore, the difference is caused

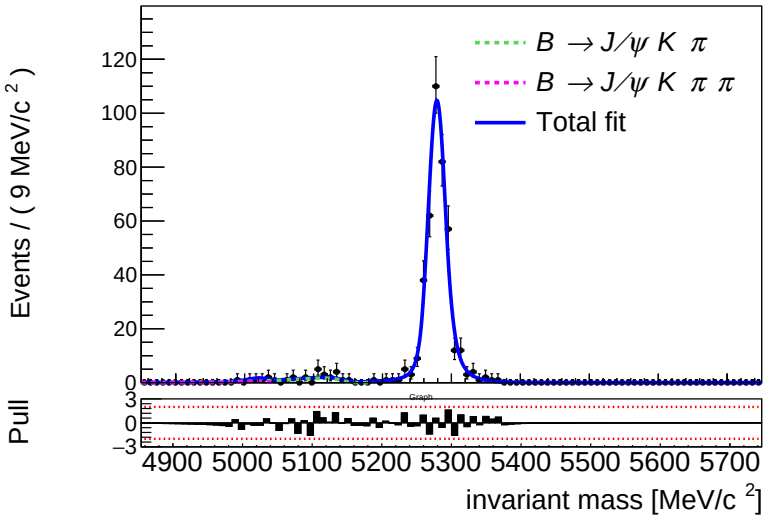

Figure 5.5: Invariant mass fit over the subset with `Bp_BpTracking_nHits>0`. Again the Gaussian peak with power-law tails is not included for clarity. The background is not shown either as its contribution is negligible.

by efficiency of the reconstruction itself. Neither the detector nor the BTracking tool is expected to capture all events and as such, this is considered a positive result.

Finally, the observed yields allow for an upper limit to be set on the expected combinatorial background for a $B^+ \to J/\psi(\to \mu^+\mu^-) \to K^+$ analysis. Although B-Tracking is not expected to improve an analysis of this kind in any way, the result is representative for combinatorial background suppression in other b-meson decays. The upper limit is expressed relative to the signal yield:

$$\frac{N_b}{N_s} < 0.37\% \quad \text{(90\% CL)}.$$

Where the 90% confidence limit is obtained by taking 1.645 standard deviation of the fraction. Compared to the signal and background yields that made it through the selection, the signal to background ratio is improved by more than a factor 250. This result promises a high purity selection with respect to combinatorics in addition to the potentially strong charmed background suppression outlined in chapter 5.

First and foremost, this chapter has demonstrated proof of principle of the BTracking tool. Demonstrating that the tool works as intended, is sufficiently efficient and also functions as an effective combinatorial background filter surpasses initial expectations.

Table 5.1: Results from simulation and data. $\eta_{BTracking}$ presents the relative number of candidates passing one VELO sensor, while η_{reco} stands for the reconstruction efficiency relative to the number of events that passed a VELO sensor.

	Simulation	Data
N_{all}	$6,381,361$	$957,362 \pm 1.406$
N_{VELO}	$3,913$	408 ± 30
$\eta_{BTracking}$	0.061%	$0.043 \pm 0.003\%$
η_{reco}	100%	$73 \pm 5\%$

Table 5.2: Cuts applied to the dataset simulated in RapidSim. FD stands for flight distance and IP stands for impact parameter, i.e. the shortest distance from the track to the PV.

Particle	Cut	
B^+	PT > 500MeV/c,	FD > 0.7mm
Muon	PT > 300MeV/c,	IP > 0.03mm
Kaon	PT > 225MeV/c,	IP > 0.03mm

Fitting the first dataset has demonstrated how RooFit works, and how the use of sWeights enables the extraction of information of individual components of a mixed dataset. This weighing can consequently be applied to a signal dataset containing both B^+ and B_c^+ decays in order to study either type separately and check B-Tracking results with a B^+ control channel. The second invariant mass fit has established that BTracking works when reconstructing real data, and has revealed an efficiency consistent with initial expectations.

Conclusion and Outlook

The Standard Model of particle physics is not the entire story. Its predictive power has impressed many and the tests it has endured, many more. But, problems have emerged that indicate the limits of the Standard Model. A number of measurements from the heavy flavour sector of particle physics have indicated that we might have arrived at a limit of the model. The Standard Model predicts that nature treats all lepton flavours equally. Measurements from the LHCb collaboration and *B-Factory* accelerators together show compelling evidence for the violation of lepton flavour universality. This thesis has been an attempt to contribute to the resolution of this issue.

The study explores the feasibility of analyzing the $B_c^+ \to \nu_\tau \tau^+ (\to \pi^+\pi^-\pi^+\overline{\nu}_\tau)$ decay mode that has not yet been observed. To achieve this goal, a novel track reconstruction tool—B-Tracking—is used that infers track directions of very short-lived particles. The question whether an analysis of this decay channel could prove worthwhile, can be answered with a resounding 'yes'. In chapter 3, it has been discussed what yields and efficiencies can be expected of the signal channels as well as background channels. The numbers are small but in principle sufficient for an analysis, due to the low efficiency of B-Tracking. The benefit of the stringent cut that B-Tracking constitutes, is the suppression of background events. Lighter *c*-mesons decays are likely to pass that cut. In chapter 4, a selection strategy has been spelled out to effectively contain charmed background modes. Chapter 5 has investigated the effect of B-Tracking on combinatorial effects in real run 2 data. Although the amount of data is limited, no combinatorial background events have been observed when a B-Tracking hit is required.

The preliminary results paint a promising picture. They are only a start, however. The next steps to be taken are necessary to make a more robust case in favour of a B-Tracking analysis, and to ensure that the LHCb experiment is prepared for the analysis. The first step should be to generate a dataset with the full LHCb simulation suite of the signal decay modes, rather than RapidSim datasets. The initial efficiencies can then be cross-checked. With the simulation of background events, the efficiency of the selection procedure can also be determined more accurately. Once the kinematics of the signal are understood in more detail, a trigger line can be written to ensure VELO data of signal

events is stored. The challenge is to retain as much of the signal as possible, while keeping the required bandwidth in check.

Only when run 3 of data taking at the LHC is underway, can the study presented here begin to bear fruit. The analyses of the two signal decay modes will not be similar, and neither will the impact. The $B^+ \to \nu_\tau \tau^+ (\to \pi^+\pi^-\pi^+\overline{\nu}_\tau)$ decay is much more numerous, but whether the results are competitive remains to be seen. The $B_c^+ \to \nu_\tau \tau^+ (\to \pi^+\pi^-\pi^+\overline{\nu}_\tau)$ mode on the other hand will be seen much less, but the potential results are much more significant. Measuring a fully leptonic B_c^+ decay is moving into uncharted waters.

The feasibility of an analysis with b-meson tracking has been approached from different sides. Every time it has yielded positive results. As such, the author strongly beliefs this work should be carried on to push the capabilities of the LHCb experiment to their limit and in doing so perhaps help resolve the issue of lepton flavour universality.

Bibliography

[1] J. Horgan. *The End of Science: Facing the Limits of Knowledge in the Twilight of the Scientific Age*. Helix Books. Broadway Books, 1997. ISBN: 9780553061741.

[2] Sheldon L. Glashow. "Partial-symmetries of weak interactions". In: *Nuclear Physics* 22.4 (1961), pp. 579–588.

[3] Laurent Canetti, Marco Drewes, and Mikhail Shaposhnikov. "Matter and antimatter in the universe". In: *New Journal of Physics* 14.9 (Sept. 2012), p. 095012.

[4] S F King. "Neutrino mass models". In: *Reports on Progress in Physics* 67.2 (Dec. 2003), pp. 107–157.

[5] Aaij R. et al. "Measurement of the Ratio of Branching Fractions $\mathcal{B}(\overline{B}^0 \to D^{*+}\tau^-\overline{\nu}_\tau)/\mathcal{B}(\overline{B}^0 \to D^{*+}\mu^-\overline{\nu}_\mu)$". In: *Phys. Rev. Lett.* 115 (11 Sept. 2015), p. 111803.

[6] Werner Heisenberg. *Physics and Philosophy*. New York: Harper, 1958.

[7] J. Morrison. *Modern Physics: for Scientists and Engineers*. Elsevier Science, 2009. ISBN: 9780123859112.

[8] Elena Graverini. "Flavour anomalies: a review". In: *Journal of Physics: Conference Series* 1137 (Jan. 2019).

[9] W. Buchmüller, R. Rückl, and D. Wyler. "Leptoquarks in lepton-quark collisions". In: *Physics Letters B* 191.4 (1987), pp. 442–448. DOI: https://doi.org/10.1016/0370-2693(87)90637-X.

[10] Bhubanjyoti Bhattacharya et al. "Simultaneous explanation of the $R_{K^{(*)}}$ and $R_{D^{(*)}}$ puzzles: a model analysis". In: *Journal of High Energy Physics* 2017.1 (Jan. 2017).

[11] Taifan Zheng et al. "Analysis of Bc at CEPC". In: *Chinese Physics C* 45.2 (Jan. 2021). DOI: 10.1088/1674-1137/abcf1f.

[12] Sébastien Descotes-Genon and Patrick Koppenburg. "The CKM Parameters". In: *Annual Review of Nuclear and Particle Science* 67.1 (Oct. 2017), pp. 97–127. DOI: 10.1146/annurev-nucl-101916-123109.

[13] The ATLAS Collaboration. "The ATLAS Experiment at the CERN Large Hadron Collider". In: *Journal of Instrumentation* 3.08 (Aug. 2008), S08003–S08003.

[14] The CMS Collaboration. "The CMS experiment at the CERN LHC". In: *Journal of Instrumentation* 3.08 (Aug. 2008), S08004–S08004.

[15] G. Aad et al. "Observation of a new particle in the search for the Standard Model Higgs boson with the ATLAS detector at the LHC". In: *Physics Letters B* 716.1 (Sept. 2012), pp. 1–29.

[16] The ALICE Collaboration. "The ALICE experiment at the CERN LHC". In: *Journal of Instrumentation* 3.08 (Aug. 2008), S08002–S08002.

[17] The LHCb Collaboration. "The LHCb Detector at the LHC". In: *Journal of Instrumentation* 3.08 (Aug. 2008), S08005–S08005.

[18] P.A. Zyla et al. "Review of Particle Physics". In: *PTEP* 2020.8 (2020), p. 083C01. DOI: 10.1093/ptep/ptaa104.

[19] Marzia Bordone et al. "A three-site gauge model for flavor hierarchies and flavor anomalies". In: *Physics Letters B* 779 (Apr. 2018), pp. 317–323.

[20] R. Aaij et al. "Test of lepton flavor universality by the measurement of the $B^0 \to D^{*-}\tau^+\nu_\tau$ branching fraction using three-prong τ decays". In: *Physical Review D* 97.7 (Apr. 2018).

[21] R. Aaij et al. "Search for the lepton-flavour violating decays $B^0_{(s)} \to e^{\pm}\mu^{\mp}$". In: *Journal of High Energy Physics* 2018.3 (Mar. 2018).

[22] A. Zee. *Quantum field theory in a nutshell*. Nov. 2003. ISBN: 978-0-691-14034-6.

[23] G.A. Cowan, D.C. Craik, and M. Needham. "RapidSim: An application for the fast simulation of heavy-quark hadron decays". In: *Computer Physics Communications* (Dec. 2016).

[24] Torbjörn Sjöstrand, Stephen Mrenna, and Peter Skands. "A brief introduction to PYTHIA 8.1". In: *Computer Physics Communications* 178.11 (June 2008), pp. 852–867.

[25] D. J. Lange. "The EvtGen particle decay simulation package". In: *Nucl. Instrum. Meth. A* 462 (2001). Ed. by S. Erhan, P. Schlein, and Y. Rozen, pp. 152–155.

[26] P. Golonka and Z. Was. "PHOTOS Monte Carlo: a precision tool for QED correctionsin Z and W decays". In: *The European Physical Journal C* 45.1 (Jan. 2006), pp. 97–107.

[27] J. Allison et al. "Geant4 developments and applications". In: *IEEE Transactions on Nuclear Science* 53.1 (2006), pp. 270–278.

[28] Matteo Cacciari et al. "Theoretical predictions for charm and bottom production at the LHC". In: *Journal of High Energy Physics* 2012.10 (Oct. 2012).

[29] R. Aaij et al. “Measurement of the b-Quark Production Cross Section in 7 and 13 TeV pp Collisions”. In: *Physical Review Letters* 118.5 (Feb. 2017).

[30] R. Aaij et al. “Measurements of prompt charm production cross-sections in pp collisions at s = 13 TeV”. In: *Journal of High Energy Physics* 2016.3 (Mar. 2016).

[31] F. Pedregosa et al. “Scikit-learn: Machine Learning in Python”. In: *Journal of Machine Learning Research* 12 (2011), pp. 2825–2830.

[32] T.A. Moore. *Six Ideas That Shaped Physics: Unit R - Laws of Physics are Frame-Independent*. McGraw-Hill Education, 2002. ISBN: 9780072397147.

[33] Kristof De Bruyn. “Searching for penguin footprints: Towards high precision CP violation measurements in the B meson systems”. Presented 08 Oct 2015. Apr. 2015.

[34] Ignacio Icke. “Overfitting”. In: (Feb. 2008 (accessed 2nd of Januray, 2021)). URL: https://en.wikipedia.org/wiki/Overfitting.

[35] Douglas M. Hawkins. “The Problem of Overfitting”. In: *Journal of Chemical Information and Computer Sciences* 44.1 (2004), pp. 1–12.

[36] Nicolas Kruse. “Improving upstream electron identification with bremsstrahlung identification”. July 2020.

[37] F. James and M. Roos. “Minuit - a system for function minimization and analysis of the parameter errors and correlations”. In: *Computer Physics Communications* 10.6 (1975), pp. 343–367.

[38] Wouter Verkerke and David P. Kirkby. “The RooFit toolkit for data modeling”. In: *eConf* C0303241 (2003). Ed. by L. Lyons and Muge Karagoz, MOLT007. arXiv: physics/0306116.

[39] M. J. Oreglia. “A Study of the Reactions $\psi' \to \gamma\gamma\psi$ (PhD-thesis)”. 1980.

[40] H. et al. Albrecht. “Search for hadronic b–>u decays”. In: *Physics Letters B* 241.2 (May 1990), pp. 278–282.